Granular Filtration of Airborne NaCl Nanoparticles and Carbon Nanotubes

by

Chao Yan

A thesis
presented to the University of Waterloo
in fulfillment of the
thesis requirement for the degree of
Master of Applied Science
in
Mechanical and Mechatronics Engineering

Waterloo, Ontario, Canada, 2018

AUTHOR'S DECLARATION

I hereby declare that I am the sole author of this thesis. This is a true copy of the thesis, including any required final revisions, as accepted by my examiners.

I understand that my thesis may be made electronically available to the public.

Abstract

Filtration is one of the primary technologies for nanoparticle control. However, conventional filtration techniques are evaluated mostly for solid mass removal and do not show promising effectiveness for filtration of ultrafine particles. Granular beds can offer an alternative approach to remove ultrafine particles from the gas. They can offer high filtration efficiency of particles in the submicrometer.

The effects of electrostatic forces on filtration efficiency are assumed to be insignificant and neglectable since the nanoparticles are very small and the charges on them are limited. All of that is based on conventional filtration theory developed from single fiber models. However, for granular bed filters, the effects of electrostatic forces are not proved yet. The particles can take charges when they are generated and/or during their transportation. Moreover, the electrostatic forces between particles and particles, and between particles and filter media may have effects on particle transportation in the air and deposition on the surfaces of the filter media.

This work focuses on granular filtration of airborne NaCl nanoparticles and carbon nanotubes. It aims at understanding the effects of electrostatic forces on nanoparticles and to better understand the granular filtration mechanisms of single-walled carbon nanotubes.

The effect of charging was investigated using nanosized NaCl particles. The range of particles tested was about 6-250 nm in diameter under the room conditions. Three sizes of homogeneous glass beads (2, 4 and 6 mm in diameter) were used in the tests each at three media thicknesses (2.5, 7.6 and 12.7 cm), and at three flow rates (23, 45 and 65 liters per minute). The results showed that the effects of electrostatic forces had opposite effects on filtration efficiency of particles smaller and greater than 20 nm. Electrostatic forces improved the filtration efficiency of large salt particles and reduced that of smaller ones.

The granular filtration efficiency of carbon nanotubes was investigated with a straight column, and the lengths of the nanotubes were about 1- 100 μm. The granular filters were made of the same homogenous glass beads (2, 4 and 6 mm in diameter), three air face velocities of 12.0, 16.8 and 25.0 cm/s and three bed thicknesses of 10, 20 and 40 cm. Results showed the overall granular bed filtration efficiency decreases with increasing particle size, which indicated that the dominant mechanism is Brownian diffusion. The flow rates have an adverse effect on the filtration efficiency. As the bed

thickness increased, the filtration efficiency increased. And the fine granule media diameter is a favorable factor for increasing filtration efficiency.

Four theoretical models were compared with the experimental results of filtration of carbon nanotubes. The UBE model had a good agreement with the experiment results by 2 mm glass beads. And Tardos's model fitted the experiment results better by 4 mm and 6 mm glass beads.

Keywords: Nanoparticle, Granular filtration, Electrostatic forces, Nanosized NaCl particles, Carbon Nanotubes

Acknowledgements

First and foremost, I would like to express my most sincere gratitude and appreciation to my supervisor, Dr. Zhongchao Tan, who gave me the opportunity to study at University of Waterloo. I would thank him for his patience, understanding, motivation, support, and immense knowledge. He not only guides me the academic research but also give me the advice on life. Not only focused on engineering area, but he also opened a bigger window to show me the whole world. Without his guidance and persistent help, this work cannot be completed. I also would like to express my appreciation to my thesis reviewers, Dr. Jean-Pierre Hickey and Dr. Hossein Sojoudi, for their kind guidances and constructive feedbacks on my thesis.

My sincere thanks also go to my group members, Sudong, Grace, Harry, Ryan, Yiming, Fang Liu, Hesheng, Raheleh, Fangyan, Joerg, Maryam, and Haiming. The group has been a source of friendship as well as useful advice and collaboration. I cannot forget the happy moments we experienced together, and these will be my precious memories. I am also deeply thankful to the staff at the Mechanical and Mechatronics Engineering department at the University of Waterloo.

Last but not the least, I would like to thank my family and my girlfriend. I am grateful to my parents for their unconditional love, support, and great understanding. To my loving girlfriend, you have listened to my frustrations and talk me through some difficult times. Thank you for supporting me, inspiring me, understanding me and helping me putting pieces together. Without your love, I would not have made it this far.

Dedication

To my parents

To my loving girlfriend

Table of Contents

List of Figures

List of Tables

List of Symbols

Symbol	Term	Unit
A	constant in the stream function expression, Eqn (2.15)	-
a_c	collector radius (either capillary or spherical)	m
$a_i(N_e)$	approximation coefficients for Eqn (2.60)	-
a_p	particle radius	m
b	radius of Happel's cell	m
c_i	effluent particle concentration of the *ith* unit bed element	g/cm^3 or 1/cm^3
c_{i-1}	influent particle concentration of the *ith* unit bed element	g/cm^3 or 1/cm^3
c_{in}	inlet particle concentration	g/cm^3 or 1/cm^3
c_{out}	outlet particle concentration	g/cm^3 or 1/cm^3
c_s	Cunningham correction factor	-
D	diffusivity	m^2/s
$(D_{BM})_\infty$	Brownian diffusivity without hydrodynamic retardation effect	m^2/s
D_f	diameter of the granular bed	m
D_0	diameter of the circular duct carrying the flow rate of Q_0	m
D_P	diameter of the sampling probe	m
d_c	constriction diameter of a constricted tube	m
$\langle d_c \rangle$	mean value of d_c	m
d_g	collector diameter	m
$\langle d_g \rangle$	average collector diameter	m
d_{cnt}	diameter of carbon nanotubes	m
d_{max}	maximum diameter of a constricted tube	m
d_p	particle diameter	m
E^2	Stokes stream function operator	-
e	Filtration efficiency of unit bed element	-
e_i	Filtration efficiency of the *ith* unit bed element	-
F_E	electrostatic forces	N

F_{EC}	Coulombic force	N
F_{EI}	forces caused by the image charges on the particle, induced by the charges of a collector	N
F_{EM}	forces caused by the image charges on the collector, induced by the charges of a particle	N
F_{ES}	forces resulting from space charge effect	N
F_{EX}	external electric field force	N
F_{ICP}	electric dipole interaction force	N
$f(N)$	fraction of charged particles	-
f	momentum accommodation coefficient	-
g	gravitational acceleration	m/s^2
h	height of a constricted tube	m
I	mass flux over a granule	$kg/s \cdot m^2$
I_c	number of unit cell types	-
J	flux of nanoparticles	g/s or 1/s
J_D	diffusive flux of particles	g/s or 1/s
J_{end}	flux of particles removed only due to end-contact interception	g/s or 1/s
J_{side}	flux of particles removed only due to side-contact interception	g/s or 1/s
k	Boltzmann constant	J/K
L	filter thickness	m
l	Thickness of unit bed element	m^3
l_{cnt}	length of carbon nanotubes	m
m^+, m^-	ionic mass	amu
N	total number of unit bed elements	-
N_c	number of collectors (or unit cells) in a unit bed element	$1/m^2$
N_E	absolute median particle charge	C
N_e	number of the elementary charge	-
N_G	gravitational parameter	-
N_{Pe}	Peclet number	

N_R	defined as a_p/a_c or d_p/d_g	-
N_{st}	Stokes number	-
N_{sh}	Sherwood number	-
n_i	number fraction of unit cells of the *ith* type	-
P	filter penetration	-
P^{+0}	the probability of attaching the positive ion to the neutral particle	-
P^{-0}	the probability of attaching the negative ion to the neutral particle	-
P^{+-}	the probability of attaching the positive ion to the negative particle	-
P^{-+}	the probability of attaching the negative ion to the positive particle	-
p_i	penetration of the *ith* unit bed element	-
Q_p	flow rate in the probe	l/m
Q_0	flow rate in the duct	l/m
q_i	volumetric flow rate through the *ith* tube	m^3/s
r	distance between two points or radial coordinate	m
S	surface area of a granule	m^2
S_{w_i}	fraction of irreducible saturation	-
T	absolute temperature	K
U	uniform velocity entering Happel's or Kuwabara's cell	m/s
$\overline{U}$	characteristic velocity of the flow	m/s
U_0	free stream velocity	m/s
U_p	gas velocity in the probe	m/s
u_r	velocity components along r coordinates	m/s
u_s	superficial velocity	m/s
u_z	velocity components along the axial direction	m/s
u_θ	velocity components along θ coordinates	m/s
u_∞	approach velocity to a single collector	m/s

Z^+, Z^-	ion mobility	$cm^2/v.s$

Greek letters

Δc	driving force of the mass transfer process	g/cm^3 or $1/cm^3$
ε	Filter bed porosity	-
ε_{ad}	Single collector adhesion efficiency	-
ξ	porosity-dependent function	-
θ	angular coordinate	-
η_c	Single collector collision efficiency	-
$(\eta_c)_{BM}$	single collector collision efficiency due to Brownian diffusion	-
$(\eta_c)_E$	single collector collision efficiency due to electrostatic forces	-
$(\eta_c)_G$	Single collector collision efficiency due to sedimentation	-
$(\eta_c)_I$	Single collector collision efficiency due to interception	-
$(\eta_c)_{I-end}$	Single collector collision efficiency due to end-contact interception	-
$(\eta_c)_{I-side}$	Single collector collision efficiency due to side-contact interception	-
$(\eta_c)_i$	Single collector collision efficiency due to inertial impaction	-
η_{filter}	overall filter efficiency	-
η_i	single collector efficiency of the *ith* type	-
η_s	single collector efficiency	-
λ	mean free path of the fluid	m
μ	fluid viscosity	Pa·s
ρ	fluid density	Kg/m^3
ρ_p	particle density	Kg/m^3
ψ	stream function	-

Chapter 1
Introduction

1.1 Background

Air quality directly affects human life and the environment. Clean air is considered to be an essential requirement for human beings. However, with the rapid growth in population, urbanization, and industrialization, air pollution is becoming a serious problem. The adverse effects of air pollutants call for new technologies for the measurement and control of air pollution.

Major air pollutants include sulfur oxides (SO_X), nitrogen oxides (NO_X), carbon monoxide (CO), volatile organic compounds (VOCs), ground-level ozone (O_3), toxic metals, ammonia (NH_3), and particulate matter (PM). According to the United States Environmental Protection Agency (EPA), *"particulate matter(PM), also known as particle pollution, is a complex mixture of extremely small particles and liquid droplets that get into air"* [1]. PM is one of six criteria air pollutants for which EPA was required to set National Ambient Air Quality Standards (NAAQS) [2]. It is also one of the monitored pollutants in Ontario's Air Quality Monitoring System [3].

The sources of PM can be primary and secondary. Primary PM comes from both natural sources (e.g., volcanoes, dust storms, forest fires, and ocean tides) and human activities (e.g., burning of fossil fuels and constructions). Secondary PM is formed from primary pollutants which already in the air, by physical and chemical reactions in the atmosphere.

An emerging air pollutant is nanosized aerosol particles or nanoaerosol particles. Advances in nanotechnology have raised the concerns over nanoparticles as a nanosized air pollutant. Technically, nanoparticles are referred to as particles with at least one dimension in the range of 1-100 nm. All properties of nanoaerosol depend on the nanoparticle size [4]. As the sizes of nanoparticles are extremely small and approach that of gas molecules, they may behave differently from micron particles.

Among the nanoparticles, carbon nanotubes (CNTs) have become an attractive nanomaterial since they were first synthesized in 1991 [5]. There are two types of CNTs, single-walled nanotubes (SWCNTs) and multi-walled nanotubes (MWCNTs). As carbon nanotubes have unique physicochemical, mechanical, and electrical properties, which the bulk materials do not have, they are of great potential in many engineering applications, including energy storage, semiconductor devices, and conductive composite materials [6].

On the other hand, the concerns of occupational exposure to carbon nanotubes have risen because of the increase in commercial interests and subsequent mass production of CNTs. Several studies have shown that carbon nanotubes exhibit adverse effects to humans and animals [7-9]. Other researchers found that CNTs were much more toxic than carbon black and quartz when they reached the lungs; CNTs could also cause serious occupational health hazards for workers [10]. For example, a study showed that inhalation exposure to MWCNTs could promote the growth of lung adenocarcinoma [11].

1.2 Motivation

Air filtration is the simplest and most widely used approach to the removal of particles from the air. Conventional filtration technologies were evaluated mostly for solid mass removal without considering the ultrafine particles, which contributes to negligible mass. The wet scrubbers have usually been used for removing particles larger than 1 μm [12]. However, they need large water consumption to compensate for the loss during operation and may result in water pollution. Electrostatic precipitators are very expensive and are failing in the filtration of submicrometer and high-resistivity particles. Fibrous filters are effective in filtration of ultrafine particles. However, they are not suitable for treating high-temperature and/or corrosive gaseous streams.

Granular filtration might offer an alternative solution for the separation of nanoparticles from the carrier gas. It could have a high filtration efficiency for particles in the micrometer and submicrometer [13-15]. Granular bed filters may have other technical and economic advantages for particle filtration, especially for applications in high temperature and high pressure environments [16-18]. Granular filtration can also remove corrosive and/or sticky particles with the proper granular media. The potential economic advantage is based on the fact that the granular filter may be more compact than either electrostatic precipitators or fabric filters.

For filtration of nanoparticles, the concept that the dominant mechanism for particle filtration is Brownian diffusion has been accepted widely. The effects of electrostatic forces on filtration efficiency were believed to be negligible since nanoparticles can carry very small amount of charges. All these are validated for conventional filters by the models developed from single fiber analysis. However, for a granular bed filter, they are not validated yet. The particles can take charges when they are generated and/or during their transportation. In addition, the electrostatic forces between particles and those between particles and filter media may affect particle transportation in the air and

their deposition on the surfaces of the filter media. The electrostatic forces between particles and granules may include image forces, dielectrophoresis due to collector charge, Coulomb Forces, space charge effect, Coulomb Forces due to external fields, and dielectrophoresis due to external electric fields [19].

Several studies have employed external electric fields in granular filtration to analyze the effects of electrostatic charges on the filtration of particles [20, 21]. Results from these studies have shown that electrostatic charges could alter the filtering behavior of a granular filter bed and improve its filtration efficiency. However, limited information is available on the effects of electrostatic forces on granular filtration of nanoparticles. Therefore, the effects of the electrostatic forces on granular filtration were experimentally studied in this work. The experiment results were also compared with four theoretical models.

1.3 Objectives

The ultimate goal is to better understand the granular filtration mechanisms of NaCl nanoparticles and single-walled carbon nanotubes. To achieve this goal, we accomplished the following three tasks.

1. To evaluate the effects of the electrostatic forces on NaCl nanoparticle filtration;
2. To determine the effects of flow rates, bed thicknesses and granule sizes on the filtration of SWCNTs;
3. To compare the filtration efficiencies predicted by theoretical models and measured by the experiments.

1.4 Overall structure of the thesis

There are six chapters in this thesis. Chapter 1 provides a brief overview of motivation and the objectives of the study. Chapter 2 covers the background knowledge of the properties, health effects of nanoparticles and carbon nanotubes, and state of the art in related areas of research. The basic theory of granular filtration and the literature review on the effects of electrostatic forces on nanoparticles are introduced as well.

Chapters 3 and 4 present the experimental works conducted. Presented in Chapter 3 are the experimental studies of the effects of the electrostatic forces on salt nanoparticles filtration. The filtration efficiencies of NaCl nanoparticles were measured with and without the neutralizer, respectively. The resulted differences in filtration performances showed that the electrostatic forces

could have a strong effect on nanoparticle filtration. Chapter 4 describes the experimental investigations on granular filtration of carbon nanotubes. Experiment results, data analysis and discussions about the effects of flow rates, bed thicknesses and granule sizes on filtration efficiency are also presented.

Modeling works are presented in Chapter 5. The comparisons of experiment results and various theoretical models are given in this chapter. Finally, Chapter 6 summarizes the conclusions and recommendations for future work.

Chapter 2
Literature Review

2.1 Overview

This chapter provides an overview of recent studies on the filtration of carbon nanotubes and theoretical models for granular filtration. The unique properties and a great variety of applications in science and industry were introduced first. Then the adverse health effects of nanoparticles and nanotubes on animals and the potential hazards to human health were reviewed, followed by a summary of recent studies of carbon nanotubes filtration. After that, the theory of granular filtration and four models to predict the overall granular bed filtration efficiency were introduced. In the end, the charges on the nanoparticles, charges on granular collectors and different status on nanoparticles of different sizes were reviewed to study the effects of electrostatic forces on filtration of nanoparticles.

2.2 Carbon nanotubes

2.2.1 Properties, applications, and health effects of carbon nanotubes

Carbon nanotubes (CNTs) are a class of nanomaterials composed of carbon only. CNTs have several unique size- and structure-dependent optical, electronic, magnetic, thermal, chemical, and mechanical properties [22] [23]. These exceptional properties prompt the use of CNTs in many engineering applications, such as electron field emitters, conductive plastics, semiconductor devices [24-26], chemical sensors and catalysts [27], biosensors, and medical devices [26, 28].

With the rapid development of CNTs in recent years, concerns over their potential impacts on human health have also arisen. Length dependent asbestos-like pathogenicity was observed when multi-walled carbon nanotubes (MWCNTs) were injected into the abdominal cavity of mice [29]. Murphy *et al*. examined three CNTs samples of differing lengths and found only the long CNTs samples caused acute neutrophilic inflammation in bronchoalveolar lavage at one week [30]. MWCNTs with a shorter length also caused adverse health effects on animal [9, 31], [32]. Sargent *et al.* showed that inhalation of MWCNTs promoted the growth of lung adenocarcinoma [11]. Animal toxicological evidence suggested the potential for a wide range of human health effects which could result from the exposure to CNTs. It has also been suggested that workers may be at risk for exposure to CNTs during the manufacture, handling, and cleanup of CNT materials [33, 34]. Several factors

may influence the toxicity of CNTs, including the degree of agglomeration [35], surface functionalization [36], metal content [37], and surface wall defects [38].

2.2.2 Research on filtration of carbon nanotubes

There have been some studies on filtration of carbon nanotubes. Chen *et al.* examined three different respirator filter media (two electrets and one fiberglass) for the filtration of monodisperse multi-walled carbon nanotubes (MWCNTs) of mobility diameters in the range of 20–500 nm at the face velocities of 5.3 and 10.6 cm/s [39]. They found that the MWCNTs penetrations were generally lower than those of NaCl at both face velocities for all three filters. However, the MWCNTs at the mobility sizes less than 100 nm tend to be straighter and more readily to align with the flow, which leads to a slightly higher penetration than the NaCl in the fiberglass filter at 10.6 cm/s face velocity. The single fiber theory predicted the penetrations of both particles in the fiberglass filters well for the particles below 100 nm mobility diameters, but discrepancies occurred for those above 100 nm in diameter. For the electret filters, the theory only predicted the MWCNTs penetration well for particles in the range of 20–30 nm in diameter.

Vo and Zhuang studied the penetration of MWCNTs through six commercial facepiece respirators. Two of them were NIOSH approved N95, N99, and N100. Tests were conducted at two constant flow rates of 30 and 85 liter per minute (lpm) [40]. The sizes of airborne MWCNTs were in the range of 20-10,000 nm, with 99% of the particles between 25 and 2840 nm. They found that the penetration at 85 lpm was greater than that at 30 lpm. Moreover, the most penetrating particle size through all six tested FFR models was in the range of 25–130 nm and 35–200 nm for the flow rates of 30 lpm and 85 lpm, respectively.

Wang *et al*. carried out experiments to study the penetration of airborne carbon nanotubes in the range of 100-400 nm mobility diameters through a screen filter [24]. The results showed that the CNTs penetration was less than the penetration of a sphere with the same mobility diameter, which was mainly due to the more considerable interception length of the CNTs. The experimental data were compared with the modeling results using single-fiber filtration efficiency theories. They found that the effective interception length can be approximated by the CNT aerodynamic diameter multiplying a scaling factor.

Wang conducted experiments for both spherical particles and elongated particles, such as carbon nanotubes and nanoparticle agglomerates [41]. The results showed that filtration efficiency was

higher for elongated particles compared to spheres with the same mobility. And the analysis using the filtration model for fibrous filters demonstrated that the enhanced interception effect was the major reason for this phenomenon. Further calculation using the filtration model showed that the penetration difference between spheres and agglomerates was affected by the filtration velocity, filter thickness, fiber size, and solidity. The most differentiating particle size (MDPS) decreased as the filtration velocity increased.

Seto et al. [42] experimentally studied the filtration of MWCNTs with electrical mobility diameters of 100, 200, and 300 nm by fibrous filters at various filtration velocities. Mono-mobility test aerosols were generated by the atomization of MWCNTs aqueous suspension followed by mobility classification with DMA. It was found that the 100 nm and 200nm particles contained a large fraction of multi-charged fibrous particles with a larger length. The 300nm particles were monodisperse in length, and they had lower penetration than spherical particles of the same mobility size. By analyzing the single fiber efficiency, it was found that the interception accompanied with the preferred orientation of fibrous particles was found to be the dominant mechanism for MWCNTs in this size range.

All the above research projects are for the filtration of airborne CNTs with respirators and screen filters. A limited number of studies have been devoted to the transport and filtration of CNTs through porous media. However, these studies were for CNTs in aqueous solutions instead of air, which are summarized as follows.

Liu *et al.* conducted a series of experiments using a one-dimensional column to study the mobility of MWCNTs in porous media. Tests were carried out for pore water velocities ranging over two orders of magnitude [43]. Their results demonstrated that pore water velocity strongly influenced the transport of MWCNTs. They developed a new model by incorporating a traditional colloid filtration theory in conjunction with a site-blocking term. The model was in good agreement with the experimental results obtained using quartz sand-packed column.

Jaisi and Elimelech investigated the transport of carboxyl-functionalized single-walled carbon nanotubes (SWCNTs) in columns packed with natural soil [44]. They found that SWCNTs filtration rate increased as the ionic strength of the solution increased, and physical straining governs SWCNTs filtration and transport under all the solutions investigated in the study. It was proposed that the shape and structure of SWCNTs, particularly the very large aspect ratio and highly bundled (aggregated)

state in aqueous solutions, the heterogeneity in soil particle size, porosity, and permeability, collectively contribute to straining in flow through soil media.

Jaisi *et al*. evaluated the transport and deposition of carboxyl functionalized SWCNTs in a well-defined porous medium composed of clean quartz sand over a range of solutions [45]. Their results showed that increasing solution ionic strength or addition of calcium ions resulted in increased SWCNTs deposition. They concluded that both physicochemical filtration and straining played roles in SWCNTs filtration at low (<3.0 mM) ionic strength, while physicochemical filtration was the dominant mechanism of SWCNTs filtration at higher ionic strengths.

Bahk et al. developed a filtration-based method and evaluated it to determine the geometrical length of carbon nanotubes, which is a significant characteristic for CNTs [46]. Airborne CNTs were generated by an atomizer, classified by a differential mobility analyzer and the geometrical length was measured by electron microscopy. It was found that the diameters of CNTs affected the relationship between the geometrical length and mobility diameter. CNTs with smaller diameters possessed longer lengths when the mobility size was fixed in the free molecular flow regime. They compared the geometrical lengths of two types of CNTs with different diameters using the models developed by Lall and Friedlander [47] and Li et al. [48]. The two models both agreed well with the measured geometrical length of both types of CNTs, which provided an approach to determine the CNTs length by the combination of mobility measurement and model calculation.

Mattison et al. [49] conducted experiments using a one-dimensional column to investigate the mobility of MWCNTs. The results showed that MWCNTs were mobile in porous media with collector sizes ranging from fine sands to silt. The increased MWCNTs filtration efficiency with decreasing collector size was likely due to the increased surface area and depositional sites.

2.3 The basic idea to predict the efficiency of granular filtration

With respect to the granular bed filters, it is usually created by filling with porous media (sands, glass beads, cotton, etc.) in a cylindrical channel with uniform cross-sectional shape, through which the dusty gas flows. The overall filter efficiency, which is the main measurable parameter of engineering interest, is defined as the ratio of particles removed by the filter to the total particles that come into the filter. It can be expressed as

$$\eta_{filter} = \frac{c_{in} - c_{out}}{c_{in}} \tag{2.1}$$

where η_{filter} is the overall filter efficiency;c_{in} is the inlet particle concentration by mass or number; c_{out} is the outlet particle concentration by mass or number.

Alternatively, the overall filter efficiency is often given in terms of penetration, *P*, which is defined as the outlet particle concentration and the inlet particles concentration ratio, $\frac{C_{out}}{C_{in}}$. Therefore, the overall filter efficiency can also be expressed as

$$\eta_{filter} = \frac{C_{in}-C_{out}}{C_{in}} = 1 - P \tag{2.2}$$

where *P* is filter penetration.

Many researchers have studied the overall granular bed filter efficiency and developed several models to calculate it [50-52]. The basic idea of predicting the overall filter efficiency is from the small element to the whole body. It assumes that every filter element (single collector) experiences similar filtration processes and acts as the very basic filter. Then, a "single collector efficiency", η_s, can be defined as *"the rate of particle collection as the fraction of the rate of particles passing through an area equal to the projected area of the collector at a plane normal to the main direction of flow and situated far enough upstream from the collector that the flow is essentially uniform"* [19]. The overall granular bed filter filtration can be viewed as the summation of all the single collector effects of filtration. Therefore, the theoretical computation of the overall filter efficiency is usually subdivided into two steps: prediction of single collector efficiency and correlating with the single element efficiency by means of a suitable macroscopic filter model [53].

Payatakes et al.[52] and Tien and Payatakes [54] developed a model for granular porous media and introduced the unit bed elements (UBE) concept to correlate the overall filtration efficiency. The homogeneous randomly packed granular bed was assumed to consist of a serious of unit bed elements (UBE) as shown in

Figure 2-1 . Each UBE was supposed to contain an assembly of collectors of specified geometry and size or size distribution or both. The sum of the efficiency of each UBE was the overall granular bed efficiency. Moreover, the efficiencies of each individual collectors determine the efficiency of the UBE.

The thickness of UBE, which is a periodic length, *l* is given by

$$l = \left[\frac{\pi}{6(1-\varepsilon)}\right]^{\frac{1}{3}} \langle d_g \rangle \tag{2.3}$$

where ε is the filter bed porosity; $\langle d_g \rangle$ is the average collector diameter.

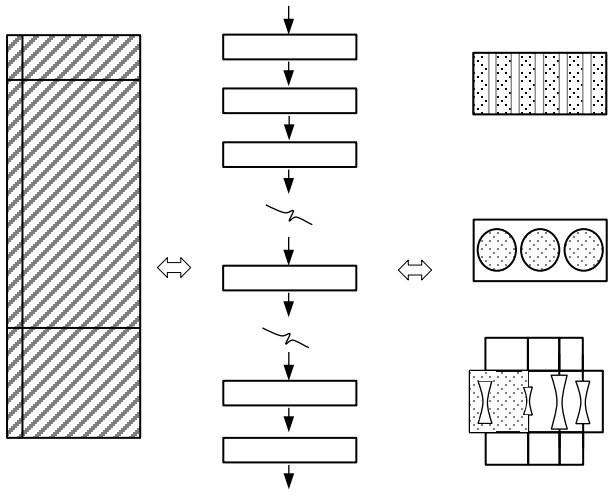

Figure 2-1 Schematic representation of granular media

2.4 Flow field of granular filtration

As mentioned in the last section, the overall granular bed filter efficiency is determined by single collector efficiency. To obtain the single collector efficiency, the flow field through the collectors must be specified. As the actual flow field is usually very complicated, a simplified model should be applied to make the calculation practicable.

For the UBE model, the granular bed filter is portrayed as a collection of UBE and each UBE consist of several individual collectors. The overall filter efficiency is obtained by each UBE efficiency which is determined by the single collector efficiency. The relationship between the UBE efficiency and the single collector efficiency must be known to obtain the overall filter efficiency. Thus, more information needs to be known, like the geometry, size, size distribution of the collectors, the number of collectors per UBE, the length of periodicity and the flow field through the collectors as well. Using appropriate porous media models can help determine these relevant parameters and complete the description of the granular bed filter.

Scheidegger [55] classified porous media models into four categories: capillary models, hydraulic radius-theory models, drag-theory models, and statistical models. For the purpose of filtration studies, Rajagopalan and Tien [56] divided porous media models into two large classes, internal flows where the fluid was assumed to flow in pores of a spatially periodic geometric structure whose walls served as particle collectors, and external flow model where the fluid was assumed to flow around the

granules. In this section, several porous media models will be introduced to get more information about the filtration process.

2.4.1 Capillary Model

Capillary model is one of the simplest internal models, which views the filter consisted of a bundle of straight capillaries of equal size, as shown in Figure 2-1. Jackson and Calvert [57] developed the capillary model for particle collection in a packed bed. When the flow inside the capillary is Poiseuillian and it can be described by the Hagen-Poiseuille law, the flow field is given by [19]

$$u_z = \frac{2u_s}{\varepsilon}\left[1 - \left(\frac{r}{a_c}\right)^2\right] \tag{2.4}$$

where u_z is the velocity components along the axial direction; u_s is the superficial velocity; r is the distance between two points; a_c is the capillary radius.

For the UBE model, the number of capillaries in each UBE, N_c is

$$N_c = \left(\frac{\varepsilon}{\pi}\right)\frac{1}{a_c^2} \tag{2.5}$$

Since all the capillaries are of the same size and particles in the flow pass through only one capillary, the UBE efficiency, e, is equal to the single collector efficiency, η_s.

2.4.2 Constricted-tube Model

Another more complicated internal model is the constricted-tube model. The concept of the constricted-tube model for porous media was first mentioned by Petersen [58]. Payatakes et al. [52] developed it and provided a formulation for the model. A packed bed is considered to consist of an array of pores. The pores at different heights are connected by the narrow channels which are called constrictions. A constricted-tube is formed by the surface of neighboring grains and two half pores joined by a constriction. The unit cell is characterized by three dimensions: the constriction diameter, d_c; the maximum diameter, d_{max}; and the height, h. These constricted-tubes are assumed to align along the direction of the main flow and have axial symmetry. Particles are deposited on the surfaces of the tubes and removed from the fluid. Due to its geometry, the filter efficiencies predicted by constricted-the tube model is higher than those by the capillary model [59].

Many investigators have offered solutions for the axisymmetrical and two-dimensional flow field with various tube geometries with the constricted-tube model. Payatakes et al.[60] provided a

numerical method for the solution of the flow field within a constricted tube of parabolic geometry. A collocation solution of the same problem but at creeping flow was given by Neira and Payatakes [61]. Fedkiw and Newman [62] presented a collocation solution for creeping flow within a sinusoidal tube. And Venkatesan and Rajagopalan [63] obtained an analytical solution for creeping flow within a hyperbolic tube.

For the constricted-tube model, the size distribution of the unit cells (constricted tube) must be specified when there are different sizes of unit cells in a UBE. The total number of the unit cells in a UBE, N_c, is [52]

$$N_c = \frac{6\varepsilon\left(1-S_{w_i}\right)\langle d_c\rangle}{\pi\langle d_c^3\rangle}\left[\frac{(1-\varepsilon)\langle d_c^3\rangle}{\varepsilon\left(1-S_{w_i}\right)\langle d_g^3\rangle}\right]^{2/3} \tag{2.6}$$

where S_{w_i} is the fraction of the irreducible saturation; $\langle d_c\rangle$ is the mean values of the pore constrictions; $\langle d_g^3\rangle$ and $\langle d_c^3\rangle$ are the mean values of d_g^3 and d_c^3.

The efficiency of the UBE, *e*, can be expressed as [19]

$$\mathrm{e} = \frac{N_c\sum_{i=1}^{I_c}(n_i q_i \eta_i)}{u_s} \tag{2.7}$$

where I_c is the number of unit cell types; n_i is the number fraction of unit cells of the *ith* type; q_i is the volumetric flow rate through the *ith* tube; η_i is the single collector efficiency of the *ith* type.

For the simple case, when all the unit cells are identical, *e* is equal to the single collector efficiency, η_s.

2.4.3 Spherical Model

In the external models, the fluid is assumed to flow around the filter element as obstacles. In most cases, the geometry of the individual collectors can be viewed as a sphere approximately. Therefore, the spherical model is used to study the granular bed filter naturally. With the assumption that the flow is considered incompressible, creeping flow and axisymmetric, the flow field around spherical collectors can be expressed as [19]

$$E^4\psi = 0 \tag{2.8}$$

where

$$E^2 = \frac{\partial^2}{\partial r^2} + \frac{\sin\theta}{r^2}\frac{\partial}{\partial\theta}\left(\frac{1}{\sin\theta}\frac{\partial}{\partial\theta}\right) \tag{2.9}$$

The velocity components, u_r and u_θ, are

$$u_r = \frac{-1}{r^2\sin\theta}\frac{\partial\psi}{\partial\theta} \tag{2.10}$$

$$u_\theta = \frac{-1}{r\sin\theta}\frac{\partial\psi}{\partial r} \tag{2.11}$$

2.4.3.1 Isolated-sphere Model

The simplest spherical model is the isolated-sphere model. It describes the UBE consisted of spherical collectors which are independent and do not take into account the mutual influence of the collectors on each other. Although it does not fit the packed bed, it may sometimes approximate the flow in a fluidized bed filter. Tardos et al. [53] summarized the solutions for the flow field around a sphere for different Reynolds numbers.

For the UBE model, the number of spherical collectors in a UBE, N_c, is [19]

$$N_c = \left[\frac{6(1-\varepsilon)}{\pi}\right]^{2/3}\langle d_g\rangle^{-2} \tag{2.12}$$

And the UBE efficiency, *e*, is [19]

$$\mathrm{e} = \frac{N_c\frac{\pi}{4}\langle d_g\rangle^2 u_\infty}{u_s}\eta_s \tag{2.13}$$

where u_∞ is the approach velocity to a single sphere.

2.4.3.2 Happel's Model

Apparently, the isolated-sphere model is too simple to describe the real flow field in an actual granular bed. The concept of the "unit cell" was proposed by Happel [64] and Kuwabara [65] to approach the flow field in a granular bed. It describes the spherical collectors as cells which consist of two parts: a solid sphere of radius a_c and a fluid envelop of radius *b* surrounding the solid sphere. The ratio of a_c and *b* is so chosen to obey the macroscopic property of the media such that

$$\frac{a_c}{b} = (1-\varepsilon)^{1/3} \tag{2.14}$$

The general solution of ψ was given by [64]

$$\psi = \mathrm{A}\left(\frac{K_1}{r^*} + K_2 r^* + K_3 r^{*2} + K_4 r^{*4}\right)\sin^2\theta \tag{2.15}$$

where

$$r^* = {}^{r}/_{a_c} \tag{2.16}$$

$$\mathrm{A} = \frac{\mathrm{U}}{2} a_c^2 = \frac{u_s}{2} a_c^2 \tag{2.17}$$

$$K_1 = {}^{1}/_{w} \tag{2.18}$$

$$K_2 = {}^{-(3+2p^5)}/_{w} \tag{2.19}$$

$$K_3 = {}^{(2+3p^5)}/_{w} \tag{2.20}$$

$$K_4 = {}^{-p^5}/_{w} \tag{2.21}$$

$$\mathrm{w} = 2 - 3p + 3p^5 - 2p^6 \tag{2.22}$$

$$\mathrm{p} = {}^{a_c}/_{b} = (1-\varepsilon)^{1/3} \tag{2.23}$$

For the UBE model, the number of spherical collectors in a UBE, N_c, is given by Eqn (2.12) and $\langle d_g \rangle$ may be taken to be [19]

$$a_c = \frac{1}{2}\langle d_g \rangle \tag{2.24}$$

And the UBE efficiency, *e*, is [19]

$$\mathrm{e} = \frac{N_c \pi b^2 u_s c_{i-1} \eta_s}{u_s c_{i-1}} = (N_c \pi b^2)\eta_c = 1.209\eta_s \tag{2.25}$$

Since the rate of flow past all the N_c collectors in the UBE, $N_c \pi b^2 u_s$, is greater than the flow rate through the UBE, u_s, it means that the collectors overlap with each other.

2.4.3.3 Kuwabara's Model

Kuwabara's model [65] is the same as Happel's model in conception and formulation. The difference between these two models is the boundary conditions applied when to obtain the solution for the flow field.

The coefficients of the stream functions Eqn (2.15) are [65]

$$\mathrm{A} = \frac{U}{2} a_c^2 \tag{2.26}$$

$$K_1 = \left(\frac{1}{2} - \frac{1}{5}p^3\right)\Big/_K \tag{2.27}$$

$$K_2 = -\frac{3}{2}\frac{1}{K} \tag{2.28}$$

$$K_3 = \left(1 + \frac{1}{2}p^3\right)\Big/_K \tag{2.29}$$

$$K_4 = -3p^3\Big/_{10K} \tag{2.30}$$

$$K = (1-p)^3\left(1 + \frac{6}{5}p + \frac{3}{5}p^2 + \frac{1}{5}p^3\right) \tag{2.31}$$

2.5 The single collector efficiency of granular filtration

The bed filtration process is particles deposition on filter media. It can be viewed as a two-step process: the transport of the particle from the fluid to the surface of the filter media and the adhesion of the particle to the surface of the filter media. The efficiency of the transport is called collision efficiency, which is defined as the ratio of the number of particles which strike the surface of the filter media and the number of the particles which flow toward the collector. The adhesion efficiency is responsible for the adhesion process and shows the fraction of particles attached to the surface of the collector. The single collector efficiency can be expressed as

$$\eta_s = \eta_c \varepsilon_{ad} \tag{2.32}$$

where η_c is the collision efficiency and ε_{ad} is the adhesion efficiency.

2.5.1 Collision Efficiency

Various physical mechanisms contribute to transporting particles from the fluid flow to the collector surfaces. The major mechanisms are inertial impaction, interception, sedimentation, Brownian diffusion, and electrostatic forces, which are responsible for the collision efficiency. These mechanisms always act at the same time, but it is convenient and useful to examine these factors individually to understand the physical meaning and significance of each mechanism.

2.5.1.1 Inertial Impaction

Inertial impaction is one of the major mechanisms for deposition of particles with diameters larger than one micron meter and without external forces in granular filtration[66]. Consider the particle-laden gas flowing over the collecting sphere. When the flow is at a distance from the collector, the

particles follow the fluid streamlines and particle trajectories are the same as the fluid streamlines. However, when the flow is approaching the collector, the fluid streamlines change directions to confirm the no-slip condition at the collector surface. At the meanwhile, the particles intend to keep the trajectories instead of coinciding with the fluid streamlines because of the inertia. The fluid streamlines and the particle trajectories change directions at the different extent, and then they deviate from each other. Some particle trajectories may intersect with the collector surface, which leads to particle intersections with the collector surfaces.

Ives [67] and Tien [66] pointed out that the characteristic parameter for the inertial effect is the dimensionless Stokes number N_{st}, which can be expressed as

$$N_{st} = \frac{2\rho_p \bar{U} a_p^2}{9\mu a_c} \tag{2.33}$$

where ρ_p is the particle density; $\bar{U}$ is the characteristic velocity of the flow; a_p is the particle radius; μ is the fluid viscosity.

This expression is suitable for the conditions that the relative motion between the particles is slight and there is no slip at the particle surface. If the particle size is comparable to the mean free path of the entraining gas molecules, significant velocity slip at the particle surface occurs. Thus, the Stokes number is defined as

$$N_{st} = \frac{2}{9} c_s \frac{\rho_p \bar{U} a_p^2}{\mu a_c} \tag{2.34}$$

where c_s is the Cunningham correction factor, given by Cunningham [68]

$$c_s = 1 + \frac{2\lambda}{d_p}(A_1 + A_2 \cdot e^{\frac{-A_3 d_p}{\lambda}}) \tag{2.35}$$

where λ is the mean free path; d_p is the particle diameter; A_1, A_2 and A_3 are experimentally determined coefficients, for air [69], $A_1 = 1.257$, $A_2 = 0.400$ and $A_3 = 0.55$.

Tien et al. [66] found that there was a critical value of the Stokes number below which particle deposition by inertial impaction was insignificant. And Ives [67] found that the inertial impaction mechanism was much more important for the air filtration than that for the liquids filtration.

Beizanie [70] provided an empirical expression for the collision efficiency resulting from inertial impaction using the isolated sphere model, which was

$$(\eta_c)_i = \frac{\beta}{1+\beta} \text{ for } N_{st} \geq 1.2130 \quad (2.36)$$

where $\beta = 0.2453(N_{St} - 1.2130)^{0.955}$

2.5.1.2 Interception

When the size of particles is very small, and all the forces acting on the particle in a fluid stream are negligible, the particle will follow the streamline and approach the collector. With the use of the isolated-sphere model, the farthest point along the collector surface where a particle can be collected is $r = a_c + a_p\,, \theta = {}^{\pi}/_{2}$.

Ives [67] gave the expression for collision efficiency due to interception, which was

$$(\eta_c)_I \cong \frac{3}{2}N_R^2 = \frac{3}{2}\left(\frac{d_p}{d_g}\right)^2 \quad (2.37)$$

Yao et al. [50] obtained the same expression by solving the mass balance equation for an isolated spherical collector. When Happel's model was used, the situation was similar. Rajagopalan and Tien [71] obtained the expression for Happel's model using the trajectory analysis. The collision efficiency due to interception is

$$(\eta_c)_I = \frac{3}{2}A_s(1-\varepsilon)^{\frac{2}{3}}N_R^2 \quad (2.38)$$

where

$$A_s = 2(1-p^5)/w \quad (2.39)$$

Interception is an important deposition mechanism in the absence of significant external forces and when the inertial impaction is negligible.

Yao et al. [50] and Rajagopalan and Tien [71] developed the expression for the collision efficiency due to interception based on the assumption that the particles are spherical. However, the length of nanotubes is much larger than their diameters. Thus, nanotubes could be viewed as cylinders. For interception, two cases should be considered: either the end or the side of the MWCNTs cylinder makes contact with the collector surface. This will be referred to as "end-contact" and "side-contact",

respectively [43], as shown in Figure 2-2.

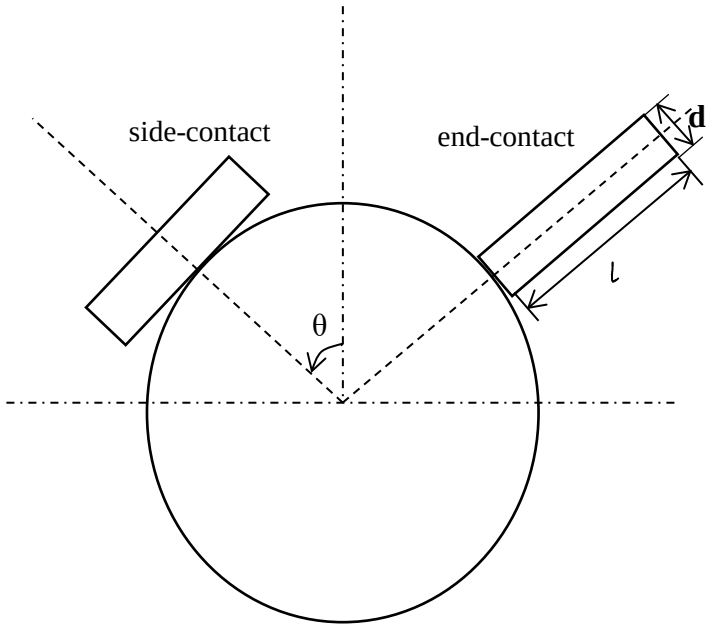

Figure 2-2 Interception mechanisms for cylindrical particles in spherical collector system

Following the procedure of Yao et al. [50], consider a spherical collector in the flow path of suspended nanoparticles. The total flux of suspended nanoparticles approaching the collector, J, can be expressed as:

$$J = U_0 c_{in} \frac{\pi d_g^2}{4} \tag{2.40}$$

Where U_0 is the free stream velocity.

The flux of MWCNTs removed only due to end-contact interception, J_{end}, can be expressed as

$$J_{end} = \frac{1}{2} U_0 c_{in} \frac{\pi {l_{cnt}}^2}{4} \left(3 - \frac{l_{cnt}}{l_{cnt}+d_g}\right) \tag{2.41}$$

Where l_{cnt} is the length of carbon nanotubes.

And the flux of MWCNTs removed only due to for side-contact, J_{side}, can be expressed as

$$J_{side} = \frac{1}{2} U_0 c_{in} \frac{\pi {d_{cnt}}^2}{4} \left(3 - \frac{d_{cnt}}{d_{cnt}+d_g}\right) \tag{2.42}$$

Where d_{cnt} is the diameter of carbon nanotubes.

By definition, the end-contact single collector efficiency of a cylindrical particle due to interception, $(\eta_c)_{I-end}$, is

$$(\eta_c)_{I-end} = \frac{J_{end}}{J} = \frac{1}{2}\left(\frac{l_{cnt}}{d_g}\right)^2\left(3 - \frac{l_{cnt}}{l_{cnt}+d_g}\right) \quad (2.43)$$

And the side-contact single collector efficiency of a cylindrical particle due to interception, $(\eta_c)_{I-side}$, is

$$(\eta_c)_{I-side} = \frac{1}{2}\left(\frac{d_{cnt}}{d_g}\right)^2\left(3 - \frac{d_{cnt}}{d_{cnt}+d_g}\right) \quad (2.44)$$

2.5.1.3 Sedimentation

If the particle density is much greater than that of the fluid, the particles will settle out in the direction of the gravity. For the isolated-sphere model, the collision efficiency due to sedimentation is [19]

$$(\eta_c)_G = \frac{2a_p^2 g(\rho_p - \rho)}{9\mu U_\infty} = N_G \quad (2.45)$$

where g is gravitational acceleration; ρ is the fluid density; N_G is the gravitational parameter.

As we see, the $(\eta_c)_G$ is given by the gravitational parameter, N_G, which is defined by using U_∞ as the characteristic velocity.

For Happel's model, $(\eta_s)_G$ is given as [19]

$$(\eta_c)_G = (1-\varepsilon)^{\frac{2}{3}} N_G \quad (2.46)$$

The values of collision efficiency due to gravitation is very small for ultrafine particles, and its effect can be negligible.

For nanotubes, the theoretical collector efficiency due to sedimentation is [43]

$$(\eta_c)_G = \left(\frac{d_{cnt}}{l_{cnt}}\right)^{\frac{2}{3}}\left\{\frac{0.146(\rho_p-\rho)g(d_{cnt}^2 l_{cnt})^{\frac{2}{3}}}{\mu U_0\left[1-\left(\frac{d_{cnt}}{l_{cnt}}\right)^2\right]^{\frac{1}{2}}}\right\}\ln\left\{\frac{1+\left[1-\left(\frac{d_{cnt}}{l_{cnt}}\right)^2\right]^{\frac{1}{2}}}{\frac{d_{cnt}}{l_{cnt}}}\right\} \quad (2.47)$$

2.5.1.4 Brownian Diffusion

For nanoparticles, the effect of the Brownian diffusion is significant. The diffusion mechanism is the result of the Brownian motion of gas molecules. Gas molecules move in random, zigzagging path and they bump the small particles in the flow. Those bumped particles start to move random and bump other particles as well, making them move in random. The smaller particle size and slower flow rates

could provide more time for particles to zigzag around. Therefore, there is a much better chance of hitting and sticking to a collector and get separated from the fluid.

In the absence of surface interaction forces, settling out of particles due to the Brownian diffusion in granular media can be considered a mass transfer process. For mass transfer in granular media, the Sherwood number N_{sh} is defined as

$$N_{sh} = \frac{d_g I}{D(\Delta c)S} \tag{2.48}$$

Where I is the mass flux over a granule; D is the diffusivity; Δc is the driving force of the mass transfer process; S is the surface area of a granule.

If the perfect sink boundary conditions are used, D may be taken to be $(D_{BM})_\infty$, which is given as

$$(D_{BM})_\infty = \frac{c_s kT}{3\pi\mu d_p} \tag{2.49}$$

where $(D_{BM})_\infty$ is Brownian diffusivity without hydrodynamic retardation effect; k is the Botlzmann constant (equal to $1.38\times10{-}23$ JK^{-1}); T is the absolute temperature.

For particle deposition, the single collector collision efficiency due to Brownian diffusion $(\eta_c)_{BM}$ may be written as

$$(\eta_c)_{BM} = \frac{4N_{Sh}}{N_{Pe}} \tag{2.50}$$

Where N_{Pe} is Peclet number, which is defined as

$$N_{Pe} = \frac{d_g u_\infty}{(D_{BM})_\infty} \tag{2.51}$$

Pfeffer and Happel [72] and Ruckenstein [73] found the Sherwood number could be expressed as

$$N_{Sh} = A_s^{1/3} N_{Pe}^{1/3} \tag{2.52}$$

By combining Eqn (2.44), the single collector collision efficiency due to Brownian diffusion is

$$(\eta_c)_{BM} = 4A_s^{1/3} N_{Pe}^{-2/3} \tag{2.53}$$

For Happel's model, the collision efficiency due to Brownian diffusion is

$$(\eta_c)_{BM} = 4(1-\varepsilon)^{2/3} A_s^{1/3} N_{Pe}^{-2/3} \tag{2.54}$$

Brownian diffusion is considered to be the dominant factor in the deposition of ultrafine particles without other forces, like electrostatic forces. Ives [67] found that the Brownian diffusion was so important for transporting the submicron size particles to the collector surface. However, the mechanism was not important for particles greater than 1 μm in diameter, since the viscous drag of the fluid restricts this movement, and the mean free path of the particle is at most one or two particle diameters [67].

For granular filtration of suspensions in liquid, nanoparticles get removed from the bulk fluid by diffusion mechanism which drives the nanoparticles across the liquid boundary layer adjacent to the collector surface. The flux across this boundary has been determined by solving the convective/diffusion equation is [74]

$$J_D = 7.98 C_{in} D^{2/3} U_0^{1/3} \left(\frac{d_g}{2}\right)^{4/3} \tag{2.55}$$

Where J_D is the diffusive flux of particles through the boundary layer to the collector. And the theoretical collector efficiency due to diffusion for the MWCNTs is[43]

$$(\eta_c)_{BM} = \frac{4.03\left\{kT ln\left[\frac{1+\left(1-\left(\frac{d_{cnt}}{l_{cnt}}\right)^2\right)^{1/2}}{\frac{d_{cnt}}{l_{cnt}}}\right]\right\}^{2/3}}{\left[3\pi\mu d_g U_0\left(\frac{3}{2}d_{cnt}^2 l_{cnt}\right)^{1/3}\left(\frac{l_{cnt}}{d_{cnt}}\right)^{2/3}\left(1-\left(\frac{d_{cnt}}{l_{cnt}}\right)^2\right)^{1/2}\right]^{2/3}} \tag{2.56}$$

2.5.1.5 Electrostatic forces

Particles may carry charges in their generation and transportation processes. In the filtration process, due to the relative motion between the granular collectors and the interactions between particles and filter media, the granular grains may be charged as well. The electrostatic charges on particles and collectors can influence particle deposition. Tardos et al. [75] showed evidence that a significant portion of the particle collection can be attributed to the electrostatic forces.

The electrostatic forces between particles and collectors are very complicated because of the many-body interactions. The simplest situation is to study a charged particle and a collector carrying charges. Kraemer and Johnstone [76] expressed the electrostatic force as

$$F_E = F_{EC} + F_{EI} + F_{EM} + F_{ES} \tag{2.57}$$

They pointed out there were four types of electric forces acting in the two-body system, which were:

1. When both the particle and the collector are charged, Coulomb Forces are applied between the particle and the collector. The force may be attractive or repulsive depending on the state of the charges on the particle and the collector, respectively. This force is denoted by F_{EC} .
2. When the collector is charged, it will induce charges which are an image opposite in sign to the collector charge on the surface of the particle, which results in an additional force on the particle. The force is denoted by F_{EI} .
3. When the particle is charged, it will induce charges which are an image opposite in sign to the particle charge on the surface of the collector, which result in an additional force on the particle. The force is denoted by F_{EM}.
4. When the particles are charged in the same sense, there will be a repulsive force among themselves. The effect is known as the space charge effect and the force is denoted by F_{ES}.

There are two more types of electrostatic forces when there is a uniform external electric field directed parallel to the flow field, the external electric field force F_{EX} and the electric dipole interaction force F_{ICP}. F_{EX} is the force between a charged particle and a neutral collector in the presence of the uniform external field. The electric dipole interaction is between a charged particle and an uncharged collector, both being polarized by the external electric field.

When all the types of electric forces are known, the collision efficiency due to electrostatic forces can be evaluated using the trajectory analysis.

2.5.1.6 The total collision efficiency

The five mechanisms mentioned above are major mechanisms for particle transportation to the surfaces of the collectors. The total collision efficiency is supposed to be the sum of these five mechanisms. Thus, the total collision efficiency for a single collector is:

$$\eta_c = 1 - [1 - (\eta_c)_i][1 - (\eta_c)_I][1 - (\eta_c)_G][1 - (\eta_c)_{BM}][1 - (\eta_c)_E] \quad (2.58)$$

If all efficiencies are small compared to unity, it can become simply

$$\eta_c = (\eta_c)_i + (\eta_c)_I + (\eta_c)_G + (\eta_c)_{BM} + (\eta_c)_E \quad (2.59)$$

2.5.2 Adhesion efficiency

Adhesion efficiency means that the ratio of the number of particles attached to the surfaces of the collectors to the number of particles which strike the surfaces of the collectors. Classical filtration

theory assumes adhesion efficiency ε_{ad} is equal to unity and that means all the particles transported to the surface of the collectors are attached to the surfaces.

When particles are extremely small, in the order of molecules size, they will behave more like molecules and less like particles. As it is known that air/gas molecules normally rebound when they hit a surface, and aerosol particles do not, there should be a critical size where particles bound off when they contact a surface.

Wang and Kasper [77] have conducted a theoretical analysis to prove the possibility of thermal rebound effect. When the particles are extremely small, they may behavior more like gas molecules rather than particles. Wang and Kasper pointed that when the impact velocity of particles exceeded the critical velocity of particles, particles would bounce off the surface. They also stated that the thermal rebound effect began at the particle size range around 10 nm and the trend of the efficiency curve for particles below 10 nm was reversed. However, it was without experimental validation.

Lots of experiments have been conducted, attempting to obtain the evidence of thermal rebound effect and the critical size. Alonso et al. [78] reported that thermal rebound on wire and tube surfaces did not occur for particles down to 2 nm. Heim et al. [79] found that no thermal rebound effect could be detected for both charged and uncharged NaCl nanoparticles in the range of 2.5-20 nm on ground metal filters and meshes, and on plastic meshes. Kim et al. [80] tested the filtration penetration of silver nanoparticles from 3 nm to 20 nm at three face velocities with four glassfiber filter media, four electret filter media, and one nanofiber filter medium. It was found that even for particles down to 3 nm, there was no significant evidence of thermal rebound. Japuntich et al. [81] conducted other experiments using NaCl and dioctyl phthalate (DOP) particles in a diameter of 10-400 nm. The results followed the classical theory of increasing filtration efficiency with decreasing particle size. The experiments conducted by Huang et al. [82] showed no thermal rebound effect occurred for NaCl particles down to 4.5 nm. Shin et al. [83] used Ag particles and a stainless steel screen mesh at an elevated temperature up to 500 k to study the effect of thermal rebound, and the results were in good agreement with the classical theory. Golanski et al. [84] also found no significant evidence of thermal rebound occurrence for graphite nanoparticles down to 10 nm. The recent work of Heim et al. [85] denoted there was no thermal rebound effect for particle diameter down to 1.2 nm.

However, other experiments found that particle penetration increased with decreasing particle diameter when particle size was smaller than 20 nm [86]. It was not clear whether the increase of penetration was caused by the thermal rebound effect indicated by Wang and Kasper [77], since

resuspension and electrostatic forces could also lead to the same effect. Therefore, there was little evidence to prove the occurrence of thermal rebound effect.

2.6 The overall granular bed filter efficiency

Many models have been proposed and they yield the following formula [87]

$$\eta_{filter} = 1 - exp\left[-\xi\eta_s\left(\frac{L}{d_g}\right)\right] \tag{2.60}$$

where ξ is the porosity-dependent function; *L* is the filter thickness.

Yao et al. [50] proposed a model to calculate the overall granular bed filter efficiency as follows

$$\eta_{filter} = 1 - exp\left[-\frac{3}{2}(1-\varepsilon)\eta_s\left(\frac{L}{d_g}\right)\right] \tag{2.61}$$

Tardos et al. [51] linked the overall filter efficiency with the single collector efficiency on the assumption that the granular bed comprised of identical collectors. The overall filter efficiency can be expressed as

$$\eta_{filter} = 1 - \exp\left[-\frac{3}{2}\frac{(1-\varepsilon)}{\varepsilon}\eta_s\left(\frac{L}{d_g}\right)\right] \tag{2.62}$$

Boulaud [88] gave another formula to calculate the filtration efficiency as

$$\eta_{filter} = 1 - exp\left[-\frac{3}{2}\varepsilon\eta_s\left(\frac{L}{d_g}\right)\right] \tag{2.63}$$

In the UBE model, for the *ith* UBE, applied the overall filter efficiency equation, the efficiency is

$$e_i = \frac{c_{i-1}-c_i}{c_{i-1}} \tag{2.64}$$

where c_{i-1} is the outlet particle concentration of the *(i-1) th* UBE, which is also the inlet particle concentration of the *ith* UBE; c_i is the outlet particle concentration of the *ith* UBE.

It also can be expressed as

$$e_i = 1 - \frac{c_i}{c_{i-1}} = 1 - p_i \tag{2.65}$$

where $p_i$is the penetration of the *ith* UBE.

Thus, the overall filter efficiency can be expressed as [19]

$$\eta_{filter} = 1 - \prod_{i=1}^{N}(1 - e_i) \tag{2.66}$$

where *N* is the total number of UBEs connected in series, which can be calculated by the equation

$$N = \frac{L}{l} \tag{2.67}$$

More precisely, *N* should be taken as the integer closest to the value of *L/l*.

2.7 Electrostatic forces on nanoparticles

The effects of electrostatic forces on filtration efficiency depend on the charges on particles and collectors. For nanoparticles, because of their small size and limited surface, the traditionary theory believes that the charges on nanoparticle are very few and the effects of electrostatic forces are limited.

2.7.1 Charges on particles

The particles can be charged during the transportation after being generated. It was believed that the distribution of the charges on particles was determined by the Boltzmann's law. However, for particles below 100 nm, some experimental results showed the distribution of the charges agreed with Fuchs's theory better [89, 90]. For particles above 100 nm, the predictions of both theories were almost the same.

For nanoaerosol particles, the analytical solution of the transient charging equation has been obtained following the Fuchs theory [91]. In this theory, he divided the space surrounding a particle into two regions. In the outer region ions move according to the continuum diffusion equation, whereas in the inner region they move as in a vacuum, it means that they have no collision with air molecules.

An approximation formula was developed according to Fuchs' theory to calculate the fraction of charged particles to avoid the complicated numerical calculations [92]

$$f(N) = 10^{\left[\sum_{i=0}^{5} a_i(N_e)(log\frac{D_p}{nm})^i\right]} \tag{2.68}$$

where *f(N)* is the fraction of charged particles; N_e is the number of elementary charge; $a_i(N_e)$ is the approximation coefficients.

The approximation coefficients can be obtained in Table 2-1. The relative errors between Fuchs's theory and this formula are less than 4% for particles less than 300 nm. This equation is valid for particles in the range of 1 nm≤d_p≤1000 nm which can take one elementary charge at most and in the

range of 20 nm≤d_p≤1000 nm which can take two elementary charges at most. For particles below 20 nm, they can carry up to one elementary charge, and for particle below about 70 nm, they can carry two elementary charges at most [92].

Table 2-1 Approximation coefficient $a_i(\mathbf{N_e})$ [92]

Approximation Coefficients $a_i(N_e)$	Number of Elementary Charge N_e				
	-2	-1	0	1	2
a_0	-26.3328	-2.3197	-0.0003	-2.3484	-44.4756
a_1	35.9044	0.6175	-0.1014	0.6044	79.3772
a_2	-21.4608	0.6201	0.3073	0.4800	-62.8900
a_3	7.0867	-0.1105	-0.3372	0.0013	26.4492
a_4	-1.3088	-0.1260	0.1023	-0.1544	-5.7480
a_5	0.1051	0.0297	-0.0105	0.0320	0.5059

The charges on particles are not only decided by the materials of the particles, but also by the generation method. Forsyth et al.[93] found that high concentration of the liquid solution could lower the charge levels.

2.7.2 Charges on granular collectors

Tardos et al. [94] observed a sharp increase in the filtration efficiency of the granular filter after the gas velocity exceeded the minimum fluidization velocity and transited from the packed bed to the fluidized bed mode. This enhancement strongly suggested that the dielectric plastic granules acquire electrostatic charges by contact or frictional electrification at the transition process from the packed bed mode to the fluidized bed mode. This phenomenon is known as triboelectrification. The filtration efficiency increase attributed to triboelectrification was also observed by Balasubramanian et al. [95] in a spouted bed filter and Figureroa and Licht [96] in packed and fluidized beds.

Liao et al. [97] carried out a series of experiments to study the effects of the vibrating conditions on the electrostatic charging of granular materials in a vertical shaker. The experiment results showed that the accumulative charges due to the interactions between collectors were very few compared to the charge accumulation due to the interactive contacts between the grains and the acrylic walls.

Moreover, the saturated electrostatic charge (absolute value) could be more than -40 nC at certain conditions. They demonstrated that the saturated accumulative charge increases with the increase of the dimensionless vibrating acceleration and decreases with increasing vibrating frequency and the saturated accumulative charge increases linearly with the increase of the vibrating velocity regardless of the vibrating frequency.

Cheng et al. [98] adopted the discrete element method to simulate the triboelectrification process in a vibrating bed. The numerical results showed that the increasing solid loading or bed diameter and decreasing granule size could lead to the increase of the charging rate in the vibrating bed.

2.7.3 Different status on particles of different sizes

Some studies have been done in charging the small and large particles. Among them, Marlow et al. [99] demonstrated that there was a significant difference in polarity between the larger and smaller ones, which passed through the same bipolar charger. In the charging process of polydisperse particles, due to unequal charging rates, large and small particles may show different polarities. Since the polarity of the collectors in the packed bed was certain, there must be a repulsive force for either large or small particles.

Tang et al. conducted experiments to study the filtration efficiency of commercial electret and discharged filter media for neutralized or singly charged nanoparticles which range from 3 to 500 nm [100]. Experimental results showed that the effects of fiber charge and particle charge on filtration performance enhancement depended on particle size. A significant improvement in efficiency for unipolarly charged particles was achieved. The filtration efficiency increased greater than 20% for particles 50–100 nm and 5–15% for particles 200–500 nm. The filtration efficiency for particles larger than ∼20 nm particles was enhanced by the polarization force. The image forces and the Coulomb Forces enhanced the collection of particles smaller than ∼100 nm and particles smaller than ∼300 nm, respectively. Charging the particles unipolarly can slow down the reduction of electrical efficiency during loading and enhance the minimum efficiency by 10–30% for 50–500 nm particles, compared to that of bipolarly charged particles.

Hoppel et al. [101] showed that for aerosols with particle sizes less than 20 nm or so the probability that a particle acquires two or more net charges of either sign is practically zero. So, there are only three different charges for aerosols below 20 nm: neutral particles, singly positive particles, and singly negative particles.

Alonso et al. [102] recalculated the ion attachment rate coefficient of Fuchs theory [91] for the particle diameter range between 2 and 20 nm with using the values of ionic mass of m^+=150 and m^- =80 amu, and ion mobilities of Z^+=1.15 and Z^- =1.65 cm^2/v.s. So, the probabilities of the ion attachments into the natural particles, positive and negative ones are as follow:

$$P^{+0} = 2.19 * 10^{-9}\, d_P^{1.51} \tag{2.69}$$

$$P^{-0} = 3.02 * 10^{-9}\, d_P^{1.51} \tag{2.70}$$

$$P^{+-} = \left(5.68 + 3.38\, d_P - 0.522\, d_P^2 + 0.042 d_P^3 - 0.0017 d_P^4 + 0.000027 d_P^5\right) * 10^{-7} \tag{2.71}$$

$$P^{-+} = \left(2.15 + 4.20\, d_P - 0.526\, d_P^2 + 0.038 d_P^3 - 0.0014 d_P^4 + 0.000020 d_P^5\right) \times 10^{-7} \tag{2.72}$$

For example, P^{+0} shows the probability of attaching the positive ion to the neutral particle. Figure 2-3 shows the probabilities of the collisions of the ions into the particles via the diameter of particles by the Alonso theory. As we can see from this chart, the probability of attachment of negative ions into positive particles is greater than the probability of attachment of positive ions into negative particles. Besides, the probability of attachment of negative ions into neutral particles is greater than the probability of attachment of positive ions into neutral particles. So at the end of the neutralizing process, negatively charged particles are predominant over positive ones for particle below about 20 nm. Since the glass beads were exposed to the atmosphere, where negative ions present. It is very likely the glass beads were already charged with negative ions. As a result, the removal efficiency for particles smaller than 20 nm was reduced because the glass beads tend to repel the incoming aerosol particles.

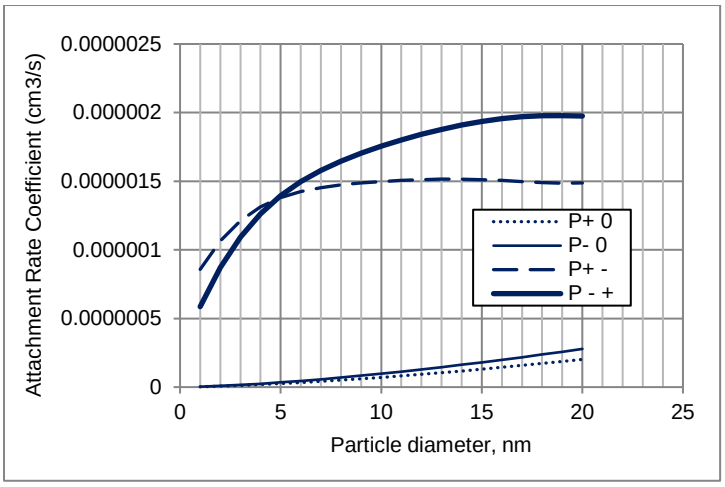

Figure 2-3 Diagram of charging probability via particle diameter by Alonso Theory

On the other hand, Christopher et al. [103] examined the positive unipolar diffusion charging in the range of 50-200 nm. He showed that particles could get more net charges by increasing the size of them. For instance, the 200 nm particle can get eleven positive ions. So, the electrostatic forces cause larger particles to be removed at high efficiency with the presence of electrostatic forces.

Thus, by the above analysis we concluded that during the process of neutralizing, small particles below 20 nm get different charges from the larger ones and because of this they have shown different behavior through the filtration. Small particles have the same charges as granules so that the electrostatic forces can have an adverse effect on filtration efficiency. On the other hand, larger particles and granules have different charges, so the electrostatic forces increase the filtration efficiency.

2.8 Summary

This chapter has reviewed the properties, applications and health effects of carbon nanotubes and the recent studies on filtration of carbon nanotubes. The theory of granular filtration and the models to predict the granular filtration efficiency have been introduced as well. The charges on the nanoparticles, charges on granular collectors and different status on nanoparticles of different sizes were discussed to study the effects of electrostatic forces on filtration of nanoparticles.

Many types of research have been carried out to study the filtration of airborne carbon nanotubes through electrets, fiberglass and screen filters. Some studies have been devoted to the filtration of carbon nanotubes through porous media in aqueous solutions. However, the studies on filtration of airborne carbon nanotubes with granular filtration are scarce. And the significance and the effects of electrostatic forces on filtration efficiency of nanoparticles are still not clear. This work aims to better understand the granular filtration mechanisms and to predict the filtration efficiency of airborne carbon nanotubes.

We carried out experiments to evaluate the significance of the effects of the electrostatic forces on salt nanoparticles filtration efficiency and discussed the effects of flow rates, bed thicknesses and granule sizes on filtration efficiencies only due to electrostatic forces, which are introduced in Chapter 3.

Chapter 4 describes the experiments used to determine the granular filtration efficiency of carbon nanotubes. The effects of flow rates, bed thicknesses and granule sizes on filtration efficiency are discussed.

Chapter 5 shows the comparisons of experimental results and various theoretical models which predicts the efficiency of granular bed filtration of carbon nanotubes.

Chapter 3
Granular Filtration of Nanosized NaCl Particles

3.1 Overview

This chapter aims to evaluate the significance of the effects of the electrostatic forces on NaCl nanoparticles filtration efficiency. This task is important and critical for the topics covered in the following chapters, which are mainly for the carbon nanotubes removal efficiency and prediction of the filtration efficiency. In order to measure the filtration efficiency only due to the electrostatic forces, the filtration efficiencies of NaCl nanoparticles were measured with and without the neutralizer, respectively.

Experimental results showed that the electrostatic forces had a significant effect on the granular filtration of NaCl nanoparticles and the effects depended on the particle size. For particles smaller than 10 nm, the effects of the electrostatic forces were negative, and for particles larger than 10 nm, the effects of the electrostatic forces were positive. The results also showed that a higher flow rate and lower bed thickness lead to higher filtration efficiency only due to electrostatic forces. The filtration efficiency only due to electrostatic forces increased with increasing particle size by 2 mm granular collectors and by larger collectors, the filtration efficiency only due to electrostatic forces had an “n” shape.

3.2 Experimental part

3.2.1 Experiment setup

The schematic diagram of the experimental set-up is shown in Figure 3-1. It includes three main sections:

1. NaCl nanoparticle generation section
2. Granular filtration section
3. Nanoparticle measurement section

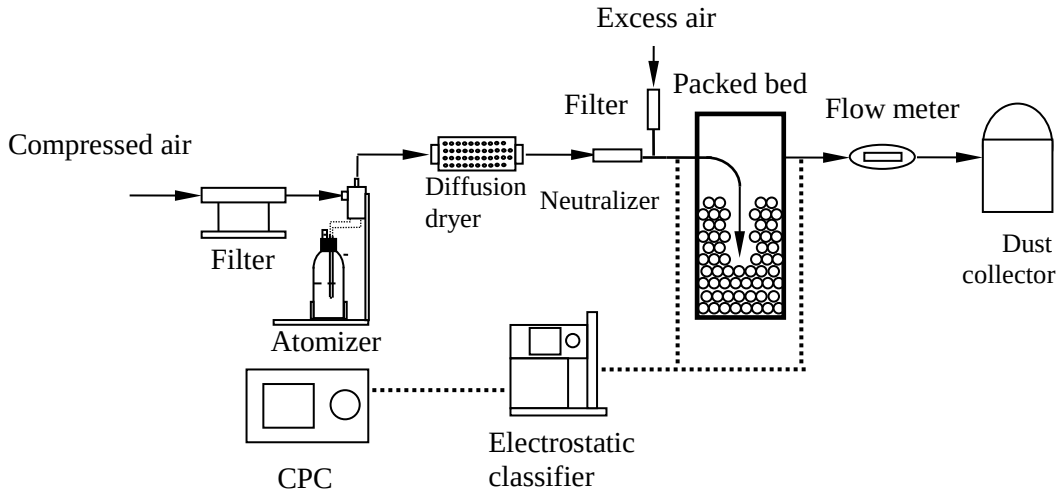

Figure 3-1 Schematic diagram of the experimental setup

The particles used in the test were polydisperse sodium chloride (NaCl) particles in the range of 6-250 nm or so, which were generated by a collision atomizer (TSI model 3076). The mean particle size changed with changing the NaCl concentration in the feed solution. In this study, the concentration was 0.1g/l, recommend by the manufacturer. After generation, the particles were dried by a diffusion dryer (TSI model 3062). And then, the particles pass through a neutralizer to eliminate electrostatic effects before getting into the packed bed.

The isokinetic sampling method was used to ensure a representative sample was taken. To guarantee the particle size distribution and concentration of sampled aerosol were similar to those of the free stream, the method required the inlet axis of sampler probe was aligned parallel to the gas streamline, and the gas velocity entering the probe was equal to the free stream velocity. The isokinetic condition for a perfectly aligned probe is

$$U_0 = U_p \tag{3.1}$$

where U_0 and U_p are the free stream velocity and the gas velocity in the probe, respectively.

To meet the condition above, the equation below should be satisfied

$$\frac{Q_p}{Q_0} = \left(\frac{D_p}{D_0}\right)^2 \tag{3.2}$$

where Q_p and Q_0 are the flow rate in the probe and in the duct, respectively; D_p is the diameter of the sampling probe; and D_0 is the diameter of the circular duct carrying the flow rate of Q_0.

In this study, the maximum flow rate was 80 lpm due to the main stream tube whose diameter was 4 cm and CPC used in the experiment. Higher main stream velocity means higher velocity in the sample probe in order to meet the criteria of the isokinetic sampling. Therefore, it needs a very small probe to provide a high velocity, which is difficult to get and easy to make particles clogged in the small inlet of probes. In addition, the CPC sampling flow rate was fixed at 1.5 lpm. Based on the available instruments and the available isokinetic sampling flow rates, the flow rates of 27, 44 and 65 lpm were used to study the effects of flow rates. The slow flow rate is to enhance the effect of diffusion which is assumed to be the dominated mechanism for nanoparticle filtration.

A thermal mass flow meter (TSI model 3063) was used to adjust the main stream flow rate to meet the criteria of the isokinetic sampling. A dust collector was used to make the system under vacuum, and an opening was provided after the aerosol generator to balance the air in the system.

3.2.2 Instruments

3.2.2.1 Particle generation system

A collision-type atomizer (TSI model 3076) was used to generate polydisperse NaCl nanoparticles. Sodium chloride was solubilized in the Deionized water (DI water) which was used as the solution. The mean particle size of the generated particles can be varied between 20 nm and 300 nm [104]. The mean particle size can change with various concentrations of the solutions. In this study, the recommended concentration, 0.1g/l was used [104].

Filtered and compressed air at no more than 240 kPa (35 psi) went through an orifice and formed a high velocity jet. The liquid was drawn to the atomizing section through a vertical passage and atomized by the air jet. Fine spray with nanoparticles left the atomizer, and the impaction on the wall removed large droplets. Extra liquid fell back to the bottle.

The atomizer was used in the conventional recirculation mode. However, the common problem of the conventional recirculation mode was reported as the evaporation of the solvent, which thickened the solution in the reservoir bottle and thus yielded larger aerosol particles. To compensate for this inconsistency, the outcome of the atomizer, which was the particle inlet concentration, was tested in every test.

3.2.2.2 Granular bed filter

Figure 3-2 shows the schematic diagram of the granular packed bed. In this experiment, a cylindrical cross-section unit was used instead of a rectangular one in order to decrease the stagnant zones. The particle-laden gas passed through the granular media of glass beads from the bottom of the bed and went upwards, forming a counter-current flow, which increased the residence time in the bed and enhanced the diffusion filtration efficiency. Although there was a 90 elbow before gas got into the packed bed, which was an obstacle for the gas flow, it was a common part in the real-world piping system. What's more, the inlet and outlet of the gas were away from each other. This structure made most of the granules near the outlet keep clean and can decrease the resuspension of particles that have been captured.

There was a fixed height which was 9 cm between the base of the filter unit and the level at which gas first interacted with the granules (h=0). This fixed thickness below h=0 was used to slow down the gas flow and acted as a flow straightener. So, the effective bed thickness was equal to an extra thickness above h=0 adding to the fixed bed thickness (9 cm). In this study, three bed thickness 2.5 cm, 7.6 cm and 12.7 cm, which are 0.1, 0.3 and 0.5 unit diameter (the diameter of the outer cylinder) above the first interaction level, were tested to study the effect of bed thicknesses on filtration efficiency. Homogenous glass beads in size 2,4 and 6 mm in diameter were used in the test. A circular mesh screen with the opening of about 1mm was installed at the outlet of the granular media to keep the granules from moving caused by the gas flow.

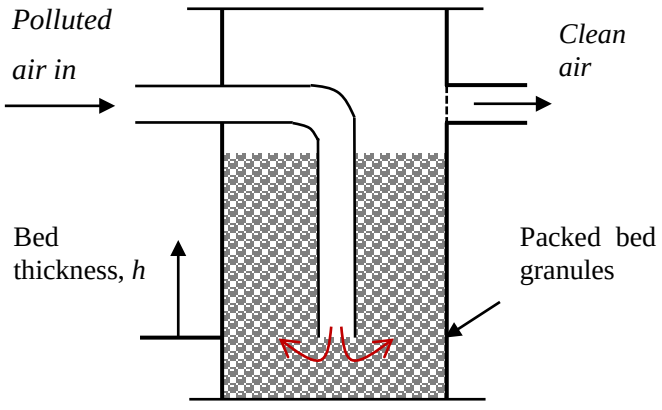

Figure 3-2 Schematic drawing of the designed packed bed

3.2.2.3 Particle measurement equipment

To determine the concentrations of particles of different diameters, an electrostatic classifier with a different mobility analyzer (DMA) was used before the condensation particle counter (CPC). The CPC obtained the concentrations of particles upstream and downstream.

3.2.3 Experimental procedure

All experiments were tested at room temperature to avoid the effect of temperature. The clean filtered air was passed through the packed bed, and the granules were purged for an hour after each set of experiments. The typical test time for each configuration was 4 minutes, and every test was conducted three times in the same conditions to get an average value of upstream concentrations of nanoparticles and downstream concentrations of nanoparticles.

The total removal efficiency was calculated as follows

$$\eta_{filter} = \frac{C_{in} - C_{out}}{C_{in}} \times 100\% \quad (3.3)$$

where c_{in} was the upstream concentration and c_{out} was the downstream concentration.

Without the neutralizer, we measured the filtration efficiencies with the electrostatic forces. Using the neutralizer, we measured the filtration efficiencies without the electrostatic forces. The differences between these two efficiencies are the filtration efficiencies only due to the electrostatic forces.

They were both measured very near to the inlet and outlet of the packed bed and could include the particles that entered the system not generated by the atomizer. However, there may be some particles captured by the granules before the system worked. So that would underestimate the efficiency of the bed. As the packed bed was purged for an hour to make the system reach a steady state before the next test operation, and the number of the resuspended particles was very small compared to the generated particles, it was expected that this case may not result in a significant effect on determining the absolute value of the filtration efficiency.

3.3 Results and discussions

3.3.1 The effect of flow rates on filtration efficiency only due to electrostatic forces

Figure 3-3 shows the results of nanosized NaCl particles filtration efficiencies only due to electrostatic forces at three filter bed thicknesses 2.5 cm, 7.6 cm and 12.7 cm at three flow rates for 2 mm glass beads. For small particles, the filtration efficiency only due to electrostatic forces is

negligible. As mentioned in Chapter 2, it is hard for small particles to be charged. And small particles can only take one or two elementary charges even if they are charged. Therefore, the electrostatic forces between particles and collectors are limited. What's more, the dominant mechanism is Brownian diffusion for smaller particles. Thus, the filtration efficiencies only due to electrostatic forces are near zero. With respect to larger particles, all the results show the filtration efficiencies only due to electrostatic forces increase with increasing particle size. As particle size increases, the particle surface where charges deposited increases as well. The charges on particles increase and the interactions between particles and collectors caused by electrostatic forces increase consequently. Adding to the decrease of the effect of Brownian diffusion as particle size increases, the effects of electrostatic forces become more significant.

From Figure 3-3 (b), the filtration efficiencies only due to electrostatic forces is negative for particles below 10 nm and positive for particles above 10 nm. The different states of charges taken by small and large particles, as mentioned in Chapter 2, may contribute to these results. The different states of charges lead to the opposite effects on filtration efficiency. However, this phenomenon is not obvious in Figure 3-3 (a) and Figure 3-3 (c).

Figure 3-3 (a) shows that the filtration efficiency only due to electrostatic forces at a slow flow rate is higher than that at a higher flow rate. The slow flow rate has a favorable effect on the effects of electrostatic forces. Particles can stay in the bed filter more time under a slow flow rate. More residence time provides more opportunities for collectors to capture the particles, which increases the filtration efficiency. However, in Figure 3-3 (b), the filtration efficiencies only due to electrostatic forces at three flow rates are almost the same, and in Figure 3-3 (c), higher flow rate leads to higher filtration efficiency only due to electrostatic forces, which is opposite to the theory. The higher flow rate helps the particles go deeper and takes more advantage of the bed under the contact level, which increases the effective bed thickness. As the bed thickness increased from 2.5 cm to 7.6 cm and 12.7 cm, the effect of higher bed thickness can compensate for the losses caused by the increase of flow rates.

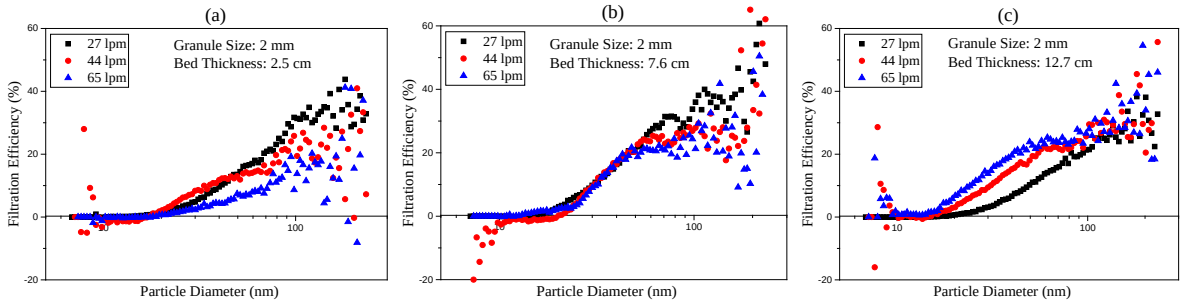

Figure 3-3 Filtration efficiency only due to electrostatic forces for 2 mm glass beads at different bed thicknesses at three flow rates

Figure 3-4 shows the results of nanosized NaCl particles filtration efficiencies only due to electrostatic forces at three filter bed thicknesses 2.5 cm, 7.6 cm and 12.7 cm at three flow rates for 4 mm glass beads. All the results show that higher flow rate leads to higher filtration efficiency only due to electrostatic forces. Besides the reason that the higher flow rate helps particles go deeper of the bed, another one is higher flow rate makes collectors move a litter more and charges due to triboelectrification between collectors increase. As the diameter of collectors increases, the bed porosity is larger, and the structure of the bed is looser than that of a bed with smaller collectors. Therefore, the collectors are easy to move. As the charges on collectors increase, the electrostatic forces increase.

In Figure 3-4 (a), we can see that the filtration efficiencies only due to electrostatic forces at 44 lpm is negative. As the process of charging nanoparticles is a probability event, there is a possibility that the particles take negative charges and the electrostatic forces have an adverse effect on filtration efficiency. At 65 lpm flow rate, the filtration efficiency only due to electrostatic forces decreases with increasing particle size. Moreover, at 27 lpm flow rate, the filtration efficiency only due to electrostatic forces increases at first and then decreases as the particle size increases. The shape of the filtration efficiency only due to electrostatic forces is “n”. The decrease of filtration efficiency only due to electrostatic forces indicates that the charges on the particles decrease as particle size increases, which is against the theory. One reason is probably that larger particles lose charges in the filtration process and another reason is maybe that the positive charges on the larger particles are neutralized by the negative charges on the small particles or ions in the air. The overall filtration efficiencies only due to electrostatic forces are still positive for larger particles.

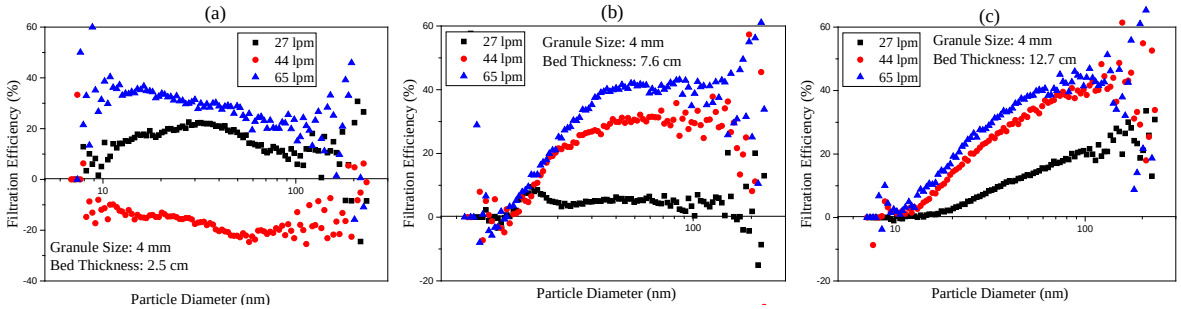

Figure 3-4 Filtration efficiency only due to electrostatic forces for 4 mm glass beads at different bed thicknesses at three flow rates

Figure 3-5 shows the results of nanosized NaCl particles filtration efficiencies only due to electrostatic forces at three filter bed thicknesses 2.5 cm, 7.6 cm and 12.7 cm at three flow rates for 6 mm glass beads. All the results show that higher flow rates lead to higher filtration efficiencies only due to electrostatic forces. The reasons have been explained above. All the filtration efficiencies only due to electrostatic forces show an "n" shape. The efficiencies increase with increasing particle size for particles below a certain size and then decreases with increasing particle size. As particle size increases, the reduction of charges on particles may result in this decrease of filtration efficiency. Another reason could be more and more particles change the state of carried charges from positive to negative. Consequently, the electrostatic forces changed from attractive forces to repulsive forces. Thus, the filtration efficiency only due to electrostatic forces decreases as increasing particle size.

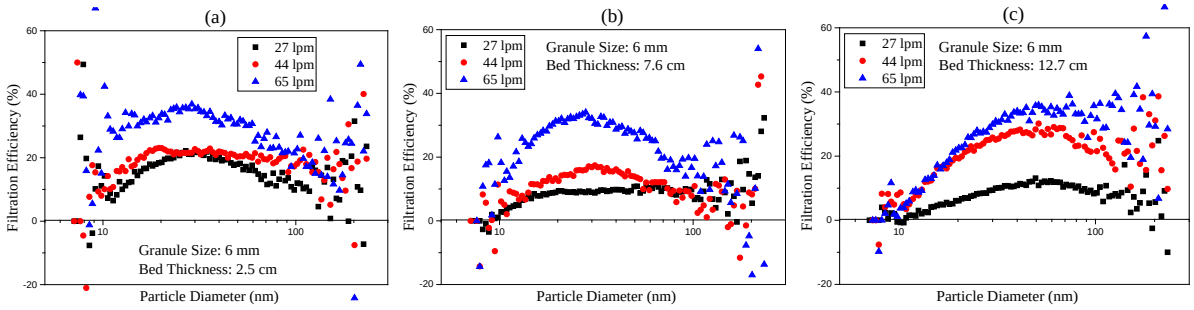

Figure 3-5 Filtration efficiency only due to electrostatic forces for 6 mm glass beads at different bed thicknesses at three flow rates

3.3.2 The effect of bed thicknesses on filtration efficiency only due to electrostatic forces

Figure 3-6 shows the results of nanosized NaCl particles filtration efficiencies only due to electrostatic forces at three filter bed thicknesses 2.5 cm, 7.6 cm and 12.7 cm at three flow rates for 2 mm glass beads. For small particles, the filtration efficiencies only due to electrostatic forces are negligible. For larger particles, all the results show the filtration efficiencies only due to electrostatic forces increase with increasing particle size.

As Figure 3-6 (c) shown, higher bed thickness provides higher filtration efficiencies only due to electrostatic forces. Higher bed thickness increases the residence time for particles to stay in the filter bed and provides more layers of collectors charged, which increases the opportunities for particles to be captured. However, Figure 3-6 (b) shows the filtration efficiencies only due to electrostatic forces for three bed thicknesses are almost the same and Figure 3-6 (a) shows that the highest bed thickness 12.7 cm has the lowest efficiency. Low flow rates and high bed thickness give the most residence time. For charged particles, they may lose charges or be neutralized by the ions in the air when they are suspended in the air for a too long time. The charged particles may be neutralized, and the effects of electrostatic forces decrease. There are two factors which act at the same time. Higher bed thickness means more residence time and more layers of collectors. However, too long residence time may lead to charged particles neutralized. Therefore, only adding the bed thickness may not increase the filtration efficiency only due to electrostatic forces for sure.

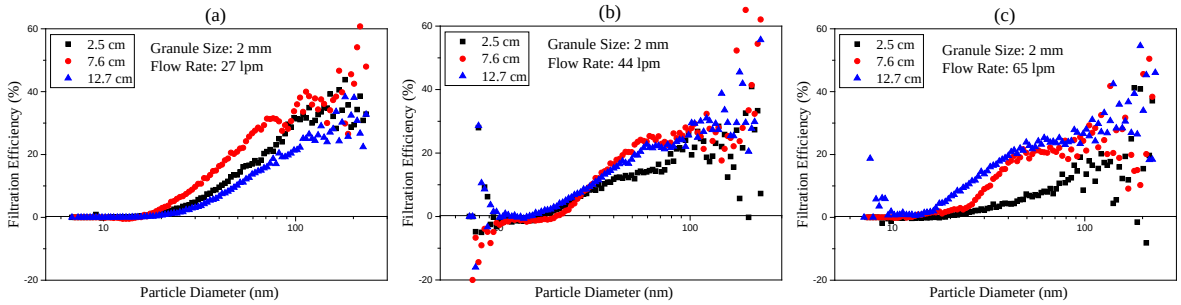

Figure 3-6 Filtration efficiency only due to electrostatic forces for 2 mm glass beads at different flow rates at three bed thicknesses

Figure 3-7 shows the results of nanosized NaCl particles filtration efficiencies only due to electrostatic forces at three filter bed thicknesses 2.5 cm, 7.6 cm and 12.7 cm at three flow rates for 4 mm glass beads. Figure 3-7 (a) shows that at 2.5 cm bed thickness, the filtration efficiency only due

to electrostatic forces increases with increasing particle size for particles below 33 nm and then decreases with increasing particle size for particles above 33 nm. For 4 mm glass beads, the bed porosity is higher than that of the bed composed of 2 mm glass beads. There are more surfaces exposed in the air, and more void space and channels for particles to pass through. Larger particles have more surfaces and are easier to take negative ions in the air. Therefore, the charged particles may be neutralized by the negative ions in the air or take negative charges. At 7.6 cm bed thickness, the filtration efficiency is lower than that at 2.5 cm bed thickness. That is maybe because there is more void space as bed thickness increases and more charged particle are neutralized. However, for 12.7 cm bed thickness, the filtration efficiency only due to electrostatic forces increases with increasing particle size.

Figure 3-7 (b) shows that at 2.5 cm bed thickness, the filtration efficiency only due to electrostatic forces is negative. That indicates that in that case, particles take negative charges which are the same as charges on the collectors. And the same charged status leads to the result that the electrostatic forces become repulsive forces. Thus, the filtration efficiency only due to electrostatic forces is negative. The filtration efficiency only due to electrostatic forces increases with increasing particle size and that at 7.6 cm bed thickness is higher than that at 12.7 cm bed thickness for particles below 40 nm.

Figure 3-7 (c) shows that filtration efficiency only due to electrostatic forces decreases with increasing particle size at 2.5 cm bed thickness. At 7.6 cm bed thickness, the filtration efficiency increases with increasing particle size and stay almost the same for particles above 38 nm.

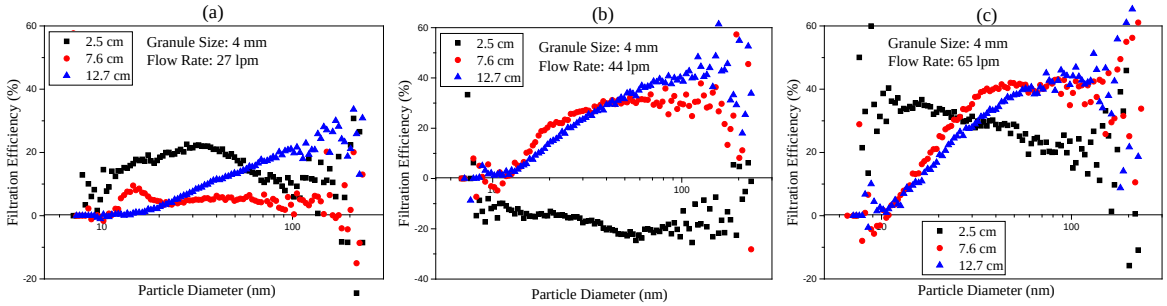

Figure 3-7 Filtration efficiency only due to electrostatic forces for 4 mm glass beads at different flow rates at three bed thicknesses

Figure 3-8 shows the results of nanosized NaCl particles filtration efficiencies only due to electrostatic forces at three filter bed thicknesses 2.5 cm, 7.6 cm and 12.7 cm at three flow rates for 6

mm glass beads. All the results have an “n” shape. Filtration efficiencies only due to electrostatic forces increase with increasing particle size and decrease with increasing particle size after they reach the summit. The filtration efficiency at 2.5 cm bed thickness is higher than that at 7.6 cm bed thickness for all three figures. The filtration efficiency only due to electrostatic forces at 12.7 cm bed thickness crosses the filtration efficiency only due to electrostatic forces at 2.5 cm and 7.6 cm bed thickness.

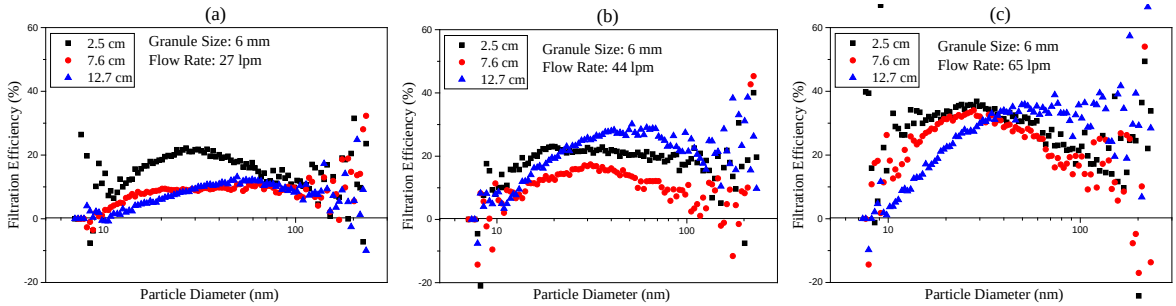

Figure 3-8 Filtration efficiency only due to electrostatic forces for 6 mm glass beads at different flow rates at three bed thicknesses

3.3.3 The effect of granule size on filtration efficiency only due to electrostatic forces

Figure 3-9 shows the results of nanosized NaCl particles filtration efficiencies only due to electrostatic forces at 2.5 cm bed thicknesses at three flow rates for 2 mm, 4 mm and 6 mm glass beads. All the three figures show that, for 2 mm glass beads, filtration efficiency only due to electrostatic forces increase with increasing particle size. For 4 mm and 6 mm glass beads, filtration efficiency only due to electrostatic forces has an “n” shape except for 4 mm glass beads at 2.5 cm bed thickness at 44 lpm. It indicates the filtration efficiency only due to electrostatic forces increases at first and decreases after it reaches the summit as particle size increases. Moreover, Figure 3-9 (a) and Figure 3-9 (c) show that for 4 mm and 6 mm glass beads, the filtration efficiencies only due to electrostatic forces are almost the same. For larger glass beads, the bed porosity is higher and there is more void space in the bed. The ions in the air may neutralize charged particles, which results in the electrostatic forces decreasing. Another reason is that for larger collectors, they are heavier than the smaller ones and harder to move. Therefore, the charges due to triboelectrification are less than those caused by the smaller glass beads. This could also explain why the electrostatic forces decrease as particle size increasing when collectors are larger.

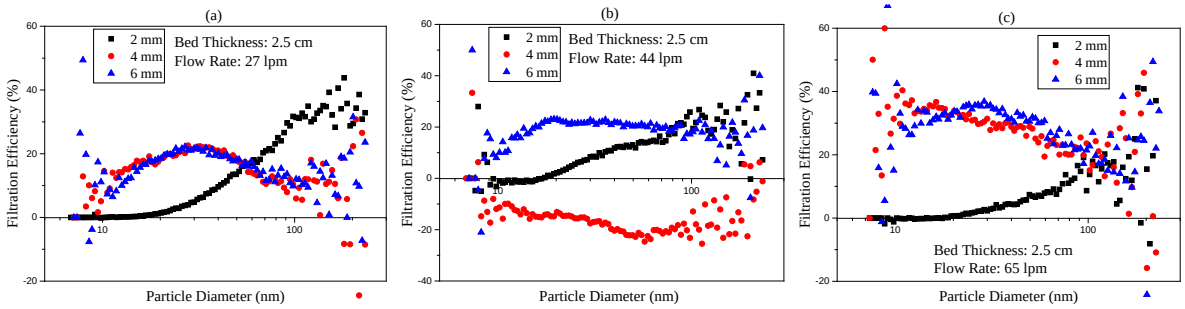

Figure 3-9 Filtration efficiency only due to electrostatic forces at 2.5 cm bed thickness at different flow rates for three glass beads

Figure 3-10 shows the results of nanosized NaCl particles filtration efficiencies only due to electrostatic forces at 7.6 cm bed thicknesses at three flow rates for 2 mm, 4 mm and 6 mm glass beads. All the three figures show that, for 2 mm glass beads, filtration efficiencies only due to electrostatic forces increase with increasing particle size. For 4 mm glass beads, the filtration efficiencies only due to electrostatic forces increase with increasing particle size at 44 lpm and 65 lpm flow rates. In the case at 27 lpm, the filtration efficiency only due to electrostatic forces increases with increasing particle size below 15 nm and decreases with increasing particle size for particles below 20 nm and stays almost the same for larger particles. For 6 mm glass beads, at 44 lpm and 65 lpm, the efficiencies have an “n” shape. At 27 lpm flow rate, the filtration efficiency only due to electrostatic forces increases with increasing particle size for particles below 20nm, and it stays almost the same for larger particles.

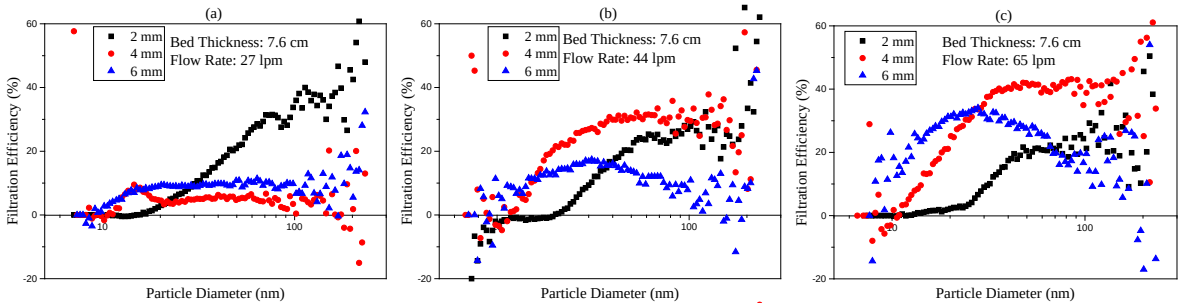

Figure 3-10 Filtration efficiency only due to electrostatic forces at 7.6 cm bed thickness at different flow rates for three glass beads

Figure 3-11 shows the results of nanosized NaCl particles filtration efficiencies only due to electrostatic forces at 12.7 cm bed thicknesses at three flow rates for 2 mm, 4 mm and 6 mm glass beads. All the three figures show that, for 2 mm and 4 mm glass beads, filtration efficiencies only due

to electrostatic forces increase with increasing particle size and the filtration efficiencies only due to electrostatic forces for 4 mm glass beads is higher than for 2 mm glass beads. That is because larger collectors have larges surfaces to carry ions in the air and take more charges than smaller collectors. Therefore, 4 mm glass beads give a stronger effect on electrostatic forces. For 6 mm glass beads, the filtration efficiencies only due to electrostatic forces have an “n” shape.

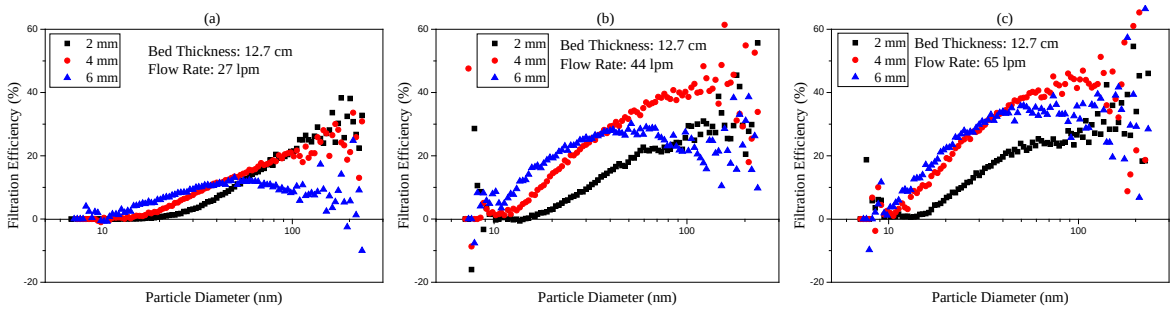

Figure 3-11 Filtration efficiency only due to electrostatic forces at 12.7 cm bed thickness at different flow rates for three glass beads

3.4 Summary

This chapter investigated the effects of the electrostatic forces on granular filtration of NaCl nanoparticles. Experiments were carried out to measure the filtration efficiencies of NaCl nanoparticles with and without the neutralizer with SMPS, respectively.

Results showed that the electrostatic forces had a significant effect on filtration efficiency and the effect was different for particles with various diameters. The electrostatic forces had a slight negative effect on filtration efficiency for particles below 10 nm. The electrostatic forces had a positive effect on filtration efficiency for larger nanoparticles, and the effects increased with increasing particle size under some conditions. High flow rates and low bed thicknesses were in favor of higher filtration efficiency only due to electrostatic forces. By 2 mm granular media diameter, the filtration efficiencies only due to electrostatic forces increased with increasing particle size. By 4 mm and 6 mm glass beads, the filtration efficiencies only due to electrostatic forces had an “n” shape. Filtration efficiencies only due to electrostatic forces increased with increasing particle size and decreased with increasing particle size after they reached the summit.

As the effects of the electrostatic forces on filtration efficiency of nanoparticles were significant, and it was difficult to measure the charges on nanoparticles and granular collectors, carbon nanotubes should be neutralized in order to eliminate the effects of the electrostatic forces, which to make sure

the experiment results could be comparable to the values calculated by the theoretical models. In the next chapter, the experiments were carried out to measure the filtration efficiency of carbon nanotubes, and the results were analyzed to show the effects of flow rates, bed thicknesses and granular media size on granular filtration of carbon nanotubes.

Chapter 4
Granular Filtration of Carbon Nanotubes

4.1 Overview

In this chapter, experiments were carried out to measure the filtration efficiency of carbon nanotubes through a vertical column filled with glass beads. With the knowledge gained in Chapter 3, the electrostatic forces have a significant effect on the filtration efficiency of nanoparticles. Thus, carbon nanotubes went through a neutralizer before they went into the granular filter. The experiment set-up was similar to the experiment set-up in Chapter 3 except the granular filter and the particle generation system. Carbon nanotubes needed to be treated as they have unique properties.

The results showed that the filtration efficiency decreased with increasing particle size, which indicated that the filtration efficiency followed the conventional theory and the dominant mechanism was Brownian diffusion. The results also showed that the slow flow rates, higher bed thickness, and finer granular media had a positive effect on filtration efficiency.

4.2 Experimental part

4.2.1 Experiment setup

The experimental set-up is shown in Figure 4-1. Airborne SWCNTs were generated by a constant output atomizer (Model 3076, TSI) from a suspension of purified SWCNTs in DI water with a concentration of 0.05 g /l. The nozzle pressure was set at 35 psi. When the atomizer was working, the SWCNTs suspension was sonicated in an ultrasonic bath (D-78224, Elma) to prevent the SWCNTs from aggregating. A diffusion dryer (Model 3062, TSI) and a Po-210 neutralizer (P-2031, NRD) were used to make the airborne CNTs dry and free of charge before entering the granular filter chamber.

The testing filter was made from packing glass beads of 2, 4 and 6 mm diameter in an acrylic column with 5 cm diameter. Circular mesh screens with the opening of about 1mm were installed at the bottom of the tube to support the glass beads and at the top of the tube to prevent the beads from moving into the duct. The collectors were packed in the tube tightly. The particle-laden gas passed through the packed bed from top to bottom. It was a simple fluid path compared to experiments in Chapter 3. Three lengths of the tube 10 cm, 20 cm and 40 cm were tested to study the effect of bed

thicknesses on filtration efficiency. With the limitations mentioned above, three flow rates 14, 19 and 29 lpm were used to study the effect of flow rates.

Concentrations of CNTs from both upstream and downstream were monitored by scanning mobility particle sizer (SMPS) which includes a differential mobility analyzer (DMA, Model 3081, TSI) and a condensation particle counter (CPC, Model 3076, TSI). An aerodynamic particle sizer (APS, Model 3321, TSI) was also used for analyzing particles with diameters from 500 nm to a few microns as SMPS can only measure between 5 nm and 500 nm. Two different face velocities of 5.9 cm/s and 2.8cm/s were selected to meet the requirement of isometric sampling. The flow rate was controlled by a mass flow meter (Model 3063, TSI) before the vacuum pump.

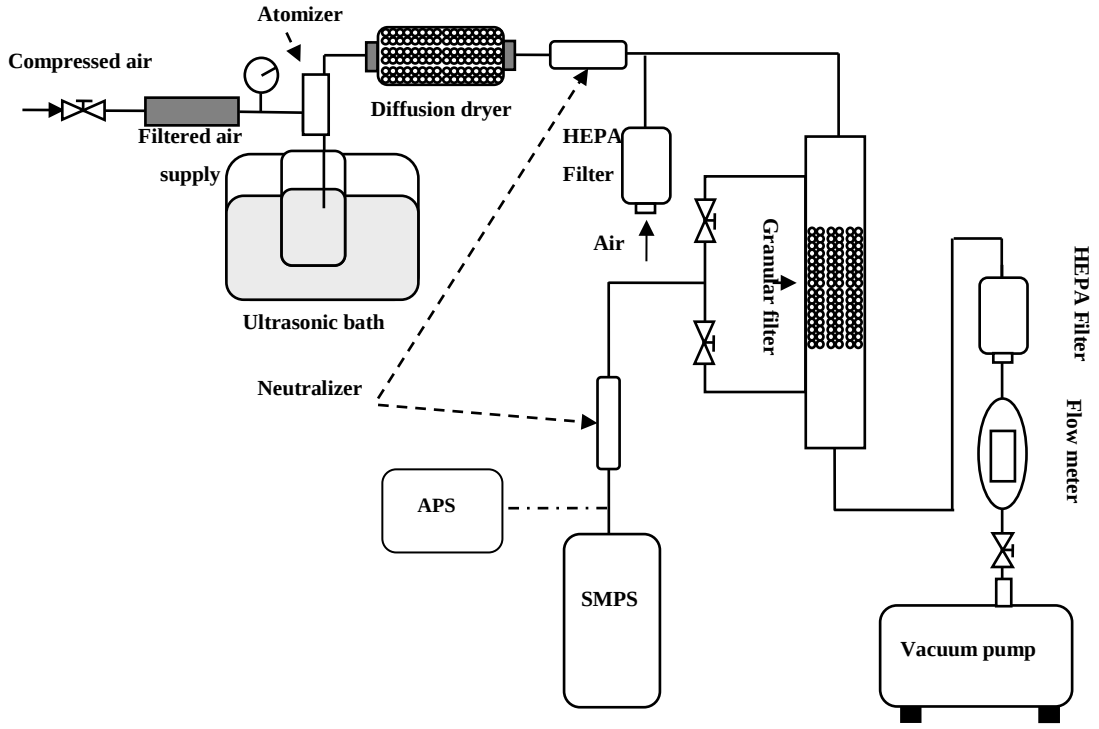

Figure 4-1 Schematic diagram of experimental setup for filtration of carbon nanotubes

4.2.2 Preparation of carbon nanotubes

The single-wall nanotubes (SWCNTs) purchased from Carbolex Inc., with purity from 50 to 70 wt% was purified by refluxing in 3 mol/L HNO_3 for 20 hours, washed with Deionized water (DI water), and then centrifuged until a neutral supernatant solution.

4.2.2.1 The SWCNTs purification

Figure 4-2 shows the suspension of purified and unpurified SWCNTs in DI water. It is very clear that the purified one has a much better dispersion in water. The 20 h reflux in 3 mol/L can partially oxidize the outer surface of SWCNTs into carboxyl groups and functionalize it with nitro functional groups. The hydrophilicity of nitro and carboxyl groups on the outer surface can be one reason for the better water dispersion of purified samples. Another reason could be the purification process can also truncate the SWCNTs from the original length of about one μm to a mean length of 200 nm. The short length reduces the chance of tangling of two individual tubes.

Figure 4-2 Picture of suspension of purified (left bottle) and unpurified (right bottle) SWCNTs in DI water

4.2.2.2 The effect of ultrasonic bath

The SWCNTs suspended in water tend to aggregate and become larger bundles. This could affect the consistency of the aerosol output from the atomizer and introduce error in our measurement. Ultrasonication is necessary to break down the bundle and make the airborne nanotube generation consistent. Figure 4-3 (a) shows the output from the atomizer with different sonication time after leaving the suspension alone for one day. The particle concentration peak value increased from 2.6×10^5 particles per ml to 3.2×10^5 particles per ml after 40 minutes of sonication. The small difference among the curves of 45, 50 and 55 minutes shown in Figure 4-3 (b) shows that 40 minutes could be enough for constant output.

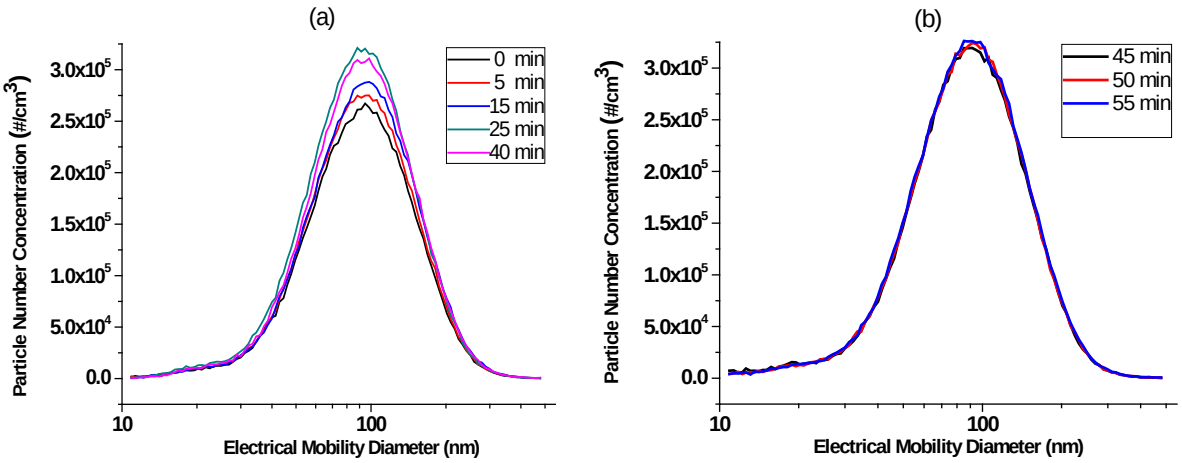

Figure 4-3 (a) The particle size distribution with different sonication time; (b)The particle size distribution with different sonication time after 40 min

4.2.3 Particle generated from Atomizer

Figure 4-4 shows the size distribution from 10 nm to 2 μm of particles generated from Constant Output Atomizer working at 240 kPa. The suspension concentration was 0.05 g/L, and the particle flow was diluted by filtered air with the total flow velocity of 12.0 cm/s. Figure 4-4 (a) shows the results measured from SMPS of the monitoring range from 10 nm to 500 nm and Figure 4-4 (b) gives the results from APS with the range from 500 nm to 2 μm. The peak of the number concentration was about 3.0×10^5 particles per ml with the particle size of about 91 nm. There were no micro size particles detected by APS although a lot of them can easily be observed within the suspension by an optical microscope. Because the high pressure from the nozzle of an atomizer could make large particles hit the wall and go back to the reservoir with the excess liquid, there was also a small peak at about 20 nm observed. This could be some impurities which cannot be removed by the purification, and the purification process can also introduce some impurities.

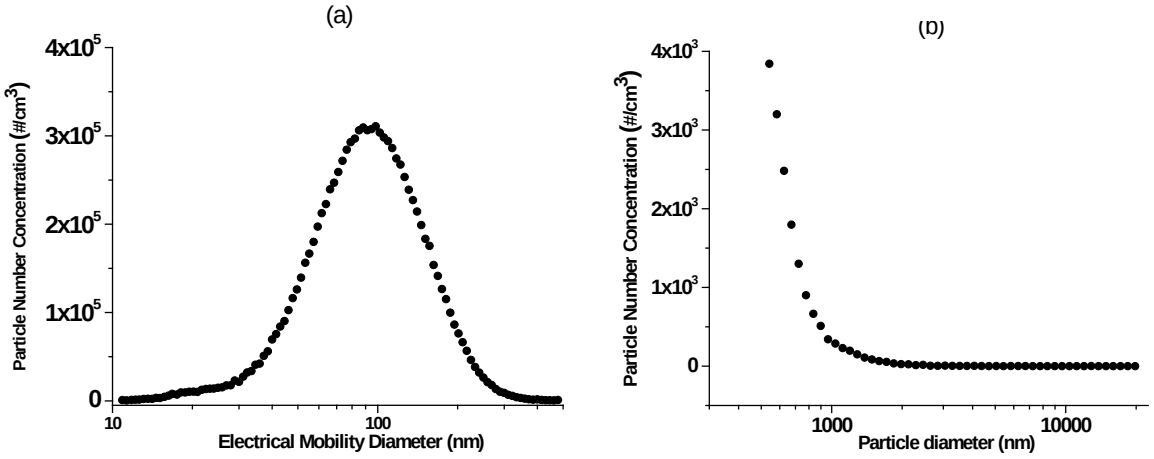

Figure 4-4 (a) The particle size distribution from atomizer measured by SMPS; (b) The particle size distribution from Atomizer measured by APS

Figure 4-5 shows the output of particles from the atomizer with the relationship of air pressure. Increase the pressure input to the atomizer increases the mean number concentration of particles but the peak position does not shift with the change of the pressure input.

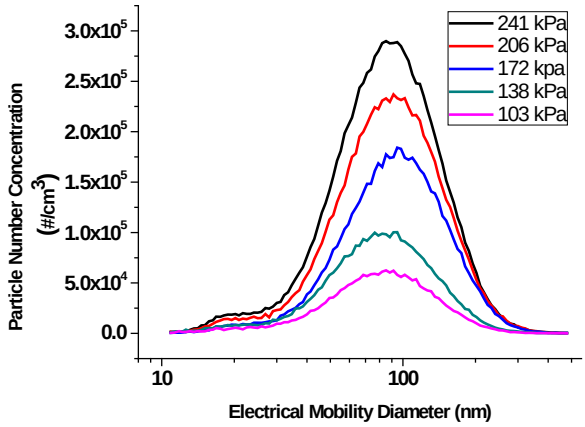

Figure 4-5 The particle size distribution from atomizer working at different pressures input

4.3 Results and discussions

4.3.1 The effect of flow rates on filtration efficiency of carbon nanotubes

Figure 4-6 shows the results of granular filtration of carbon nanotubes at three filter bed thicknesses 10 cm, 20 cm and 40 cm at three flow rates for 2 mm glass beads without the effects of electrostatic

forces. All results show that the filter efficiencies decrease with increasing particle size. The results agree with the conventional theory that Brownian diffusion is the dominant mechanism for nanosized particles. As the particle size increases, the effect of Brownian diffusion decreases, and the effects of other mechanisms do not increase very much. They cannot compensate for the loss of the efficiency due to Brownian diffusion. Therefore, the total filter efficiency decreases with increasing particle size. All the three figures show that slow flow rates lead to a higher filtration efficiency than high flow rates do. High flow rates result in less single collector efficiency according to the filtration theory mentioned in Chapter 2. It has an adverse effect on inertial impaction and interception mechanisms. In addition, high flow rates decrease the residence time of particles staying in the bed filter, which also decreases the filtration efficiency. Therefore, a slow flow rate is helpful for increasing the filtration efficiency.

Figure 4-6 (c) shows that the filtration efficiency stays at a high level for particles with a larger diameter at 40cm than that at 10 cm and 20 cm bed thickness. For small particles, Brownian diffusion is the dominant mechanism, and high bed thickness provides more residence time. The effect of Brownian diffusion has been enhanced by the high bed thickness, and the filtration efficiency can stay at a high level for larger particles. Figure 4-6 (c) also shows that the differences between the efficiencies at three flow rates are smaller than that in Figure 4-6 (a) and Figure 4-6 (b). That indicates that at high bed thickness, the effect of flow rates is not as significant as it is at low bed thickness. High bed thickness provides more opportunities for particles to be captured.

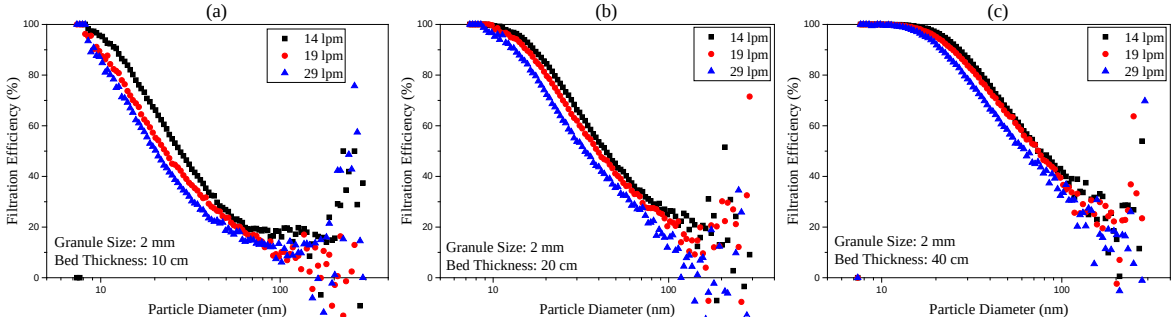

Figure 4-6 Filtration efficiency of nanotubes for 2 mm glass beads at different bed thicknesses at three flow rates

Figure 4-7 shows the results of granular filtration of carbon nanotubes at three filter bed thicknesses 10 cm, 20 cm and 40 cm at three flow rates for 4 mm glass beads without the effects of electrostatic forces. All results show that the filter efficiencies decrease with increasing particle size.

For particles above 30nm, Figure 4-7 (b) shows that the filtration efficiency at 29 lpm is the highest and the filtration efficiency at 14 lpm is the lowest. Slow flow rates could make nanotubes agglomerated to be bigger particles, which increases the filtration efficiency for small particles and decreases the filtration for bigger particles. Figure 4-7 (c) shows that for particles larger than 50 nm, the filtration efficiencies are almost the same. The effect of high bed thickness may make up the losses due to agglomeration.

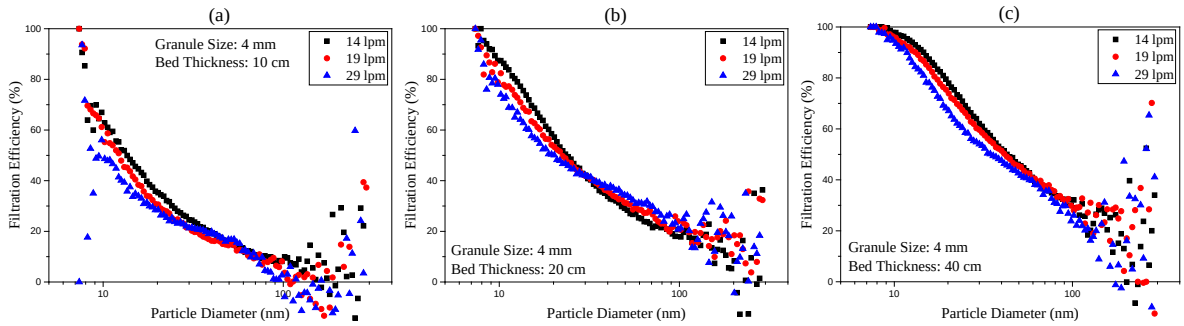

Figure 4-7 Filtration efficiency of nanotubes for 4 mm glass beads at different bed thicknesses at three flow rates

Figure 4-8 shows the results of granular filtration of carbon nanotubes at three filter bed thicknesses 10 cm, 20 cm and 40 cm at three flow rates for 6 mm glass beads without the effects of electrostatic forces. All results show that the filter efficiencies decrease with increasing particle size. As the collector diameter is bigger, the bed porosity is high, which decreases the filtration efficiency.

Figure 4-8 (b) and Figure 4-8 (c) show that for particles above 20nm, the filtration efficiency at 19 lpm flow rate is higher than the efficiencies under the other two conditions. That is also maybe the result of the effect of agglomeration. Moreover, Figure 4-8 (a) shows that three filtration efficiencies are almost the same. At low bed thickness, the residence time is short and the bigger collectors decrease the filtration efficiency. These two reasons result in all the filtration efficiencies are very low, and the differences between them are insignificant.

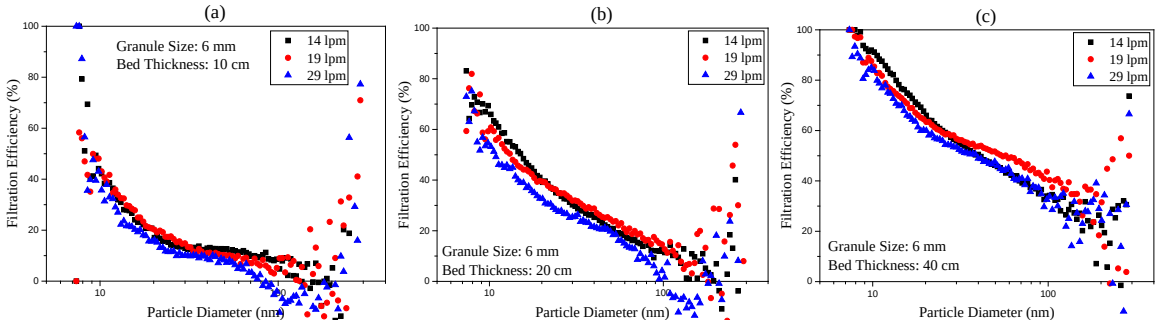

Figure 4-8 Filtration efficiency of nanotubes for 6 mm glass beads at different bed thicknesses at three flow rates

4.3.2 The effect of bed thickness on filtration efficiency of carbon nanotubes

Figure 4-9 shows the results of granular filtration of carbon nanotubes at three flow rates 14 lpm, 19 lpm and 29 lpm at three filter bed thicknesses 10 cm, 20 cm and 40 cm for 2 mm glass beads without the effects of electrostatic forces. All results show that the filter efficiencies decrease with increasing particle size. Higher bed thickness provides higher filtration efficiency. Higher bed thickness provides more residence time for particles in the bed filter and there are more layers to capture particles in the fluid. Therefore, high bed thickness has a positive effect on filtration efficiency. All three figures show that at 40 cm bed thickness, the filtration efficiencies stay at a high level for larger particle size and at 10 cm and 20 cm bed thickness, the filtration efficiencies decrease with increasing particle size. For small particles, Brownian diffusion is the dominant mechanism and the residence time is the most important factor to influence the efficiency. High bed thickness provides more residence time and compensates for the loss of the effect of Brownian diffusion due to increasing particle size.

All the three figures also show that the differences among the filtration efficiencies are almost the same under various flow rates. It is indicated that the effect of bed thickness on filtration efficiency is not influenced by the flow rates.

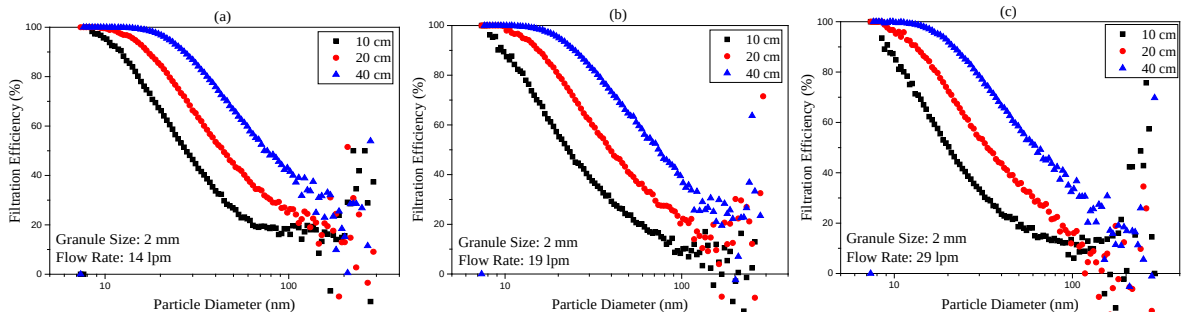

Figure 4-9 Filtration efficiency of nanotubes for 2 mm glass beads at different flow rates at three bed thicknesses

Figure 4-10 shows the results of granular filtration of carbon nanotubes at three flow rates 14 lpm, 19 lpm and 29 lpm at three filter bed thicknesses 10 cm, 20 cm and 40 cm for 4 mm glass beads without the effects of electrostatic forces. All the results show that the filter efficiencies decrease with increasing particle size. Moreover, higher bed thickness provides higher filtration efficiency. Unlike 2 mm glass beads, for 4 mm glass beads, filtration efficiencies at 40 cm decrease with increasing particles size rather than stay at a high level for small particles. Bigger collector diameter leads to high bed porosity and more void space, which allow particles to pass through the bed filter. And with the same bed thickness, bigger collector means fewer filter layers and less residence time. Therefore, at 40 cm bed thickness, the filtration efficiencies for small particles decrease with increasing particle size.

At 14 lpm and 19 lpm, the differences in filtration efficiencies are almost the same. At 29 lpm, for particles above 80 nm, the difference of filtration efficiencies between 10 cm and 20 cm bed thickness become larger, and the difference of filtration efficiencies between 20 cm and 40 cm bed thickness become smaller. That could be an experiment collecting error.

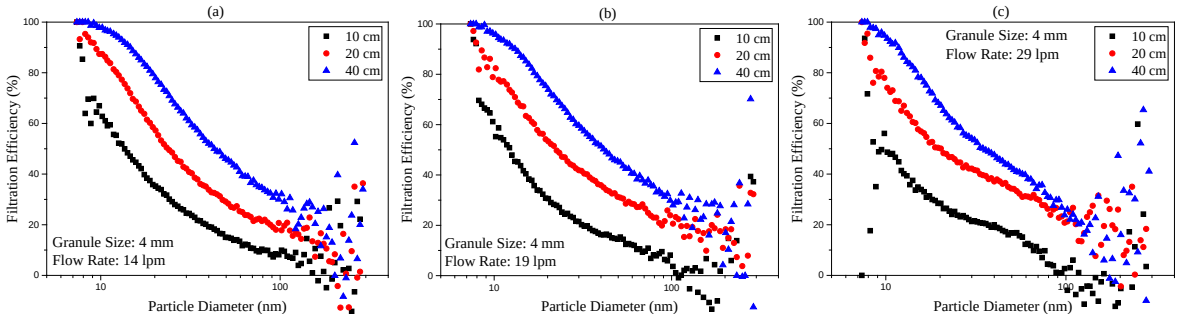

Figure 4-10 Filtration efficiency of nanotubes for 4 mm glass beads at different flow rates at three bed thicknesses

Figure 4-11 shows the results of granular filtration of carbon nanotubes at three flow rates 14 lpm, 19 lpm and 29 lpm at three filter bed thicknesses 10 cm, 20 cm and 40 cm for 6 mm glass beads without the effects of electrostatic forces. All results show that the filter efficiencies decrease with increasing particle size. Moreover, higher bed thickness provides higher filtration efficiency. All the three figures show that for particles above 40 nm, the differences of filtration efficiency between at 10 cm and 20 cm is getting smaller. The filtration efficiency at 10 cm bed thickness has reached a very low filtration efficiency for larger particles and tends to stay at that level. As the filtration efficiency at 20 cm bed thickness decreases with increasing particles, the differences between these two filtration efficiencies become smaller.

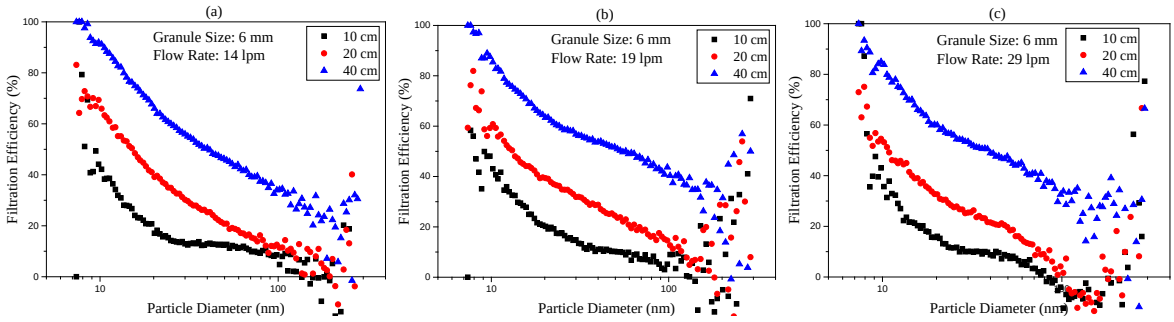

Figure 4-11 Filtration efficiency of nanotubes for 6 mm glass beads at different flow rates at three bed thicknesses

4.3.3 The effect of granule size on filtration efficiency of carbon nanotubes

Figure 4-12 shows the results of granular filtration of carbon nanotubes at 10 cm bed thickness at three flow rates 14 lpm, 19 lpm and 29 lpm for 2 mm, 4 mm and 6 mm glass beads without the effects of electrostatic forces. All results show that the filter efficiencies decrease with increasing particle

size. Moreover, a smaller collector diameter provides higher filtration efficiency. Bigger collector diameter gives higher bed porosity and more void space for particles to pass through. What's more, with the same bed thickness, bigger collector diameter means fewer layers to capture the particles in the fluid. Therefore, the bed filter consists of smaller collectors which make the bed filter more compact gives higher filtration efficiency.

All the three figures show that the differences between filtration efficiencies are getting smaller as particle diameter increases. For small particles, the Brownian diffusion is the dominant mechanism. Smaller collectors can provide smaller pores and more residence time. Thus, particles can move a less distance to reach the collector surfaces and have more opportunities to hit the collector surface. Therefore, the effect of granule size is significant for smaller particles. As particle size increases, the effect of Brownian mechanism decreases, and other mechanism did not increase very much to compensate for the loss of Brownian diffusion. All the filtration efficiencies decrease to the lowest zone, which is called "the most penetrated zone". Therefore, the differences between filtration efficiencies get smaller.

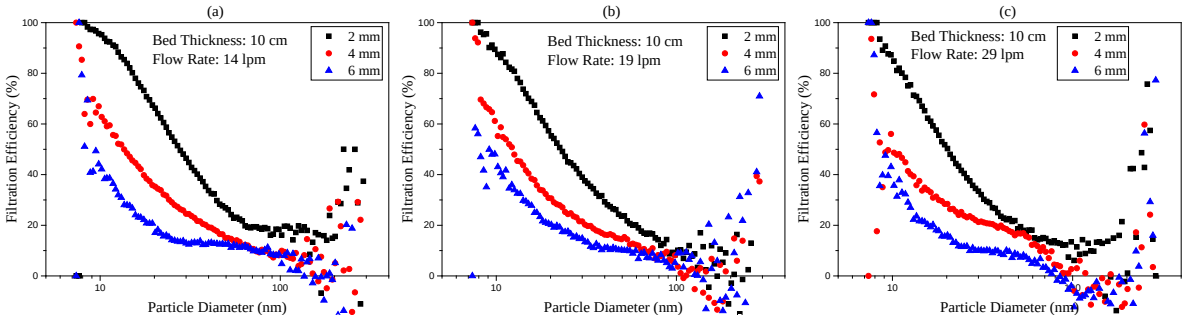

Figure 4-12 Filtration efficiency of nanotubes at 10 cm bed thickness at different flow rates for three glass beads

Figure 4-13 shows the results of granular filtration of carbon nanotubes at 20 cm bed thickness at three flow rates 14 lpm, 19 lpm and 29 lpm for 2 mm, 4 mm and 6 mm glass beads without the effects of electrostatic forces. All the results show that the filter efficiencies decrease with increasing particle size. And smaller collector diameter provides higher filtration efficiency. As the bed thickness is increased to 20 cm, higher bed thickness can compensate a part of the loss due to the decrease of the Brownian diffusion. Therefore, the differences between filtration efficiencies are not as much as that at 10 cm bed thickness. All the three figures show that the differences between filtration efficiencies are getting smaller as particle diameter increases. Figure 4-13 (c) shows that for particles above 60

nm, the filtration efficiency for 4 mm glass beads is higher than that for 2 mm glass beads. That is maybe an experimental error.

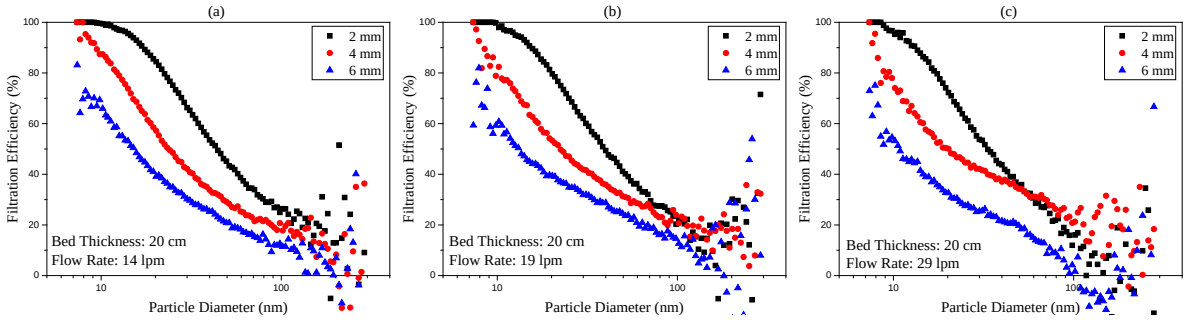

Figure 4-13 Filtration efficiency of nanotubes at 20 cm bed thickness at different flow rates for three glass beads

Figure 4-14 shows the results of granular filtration of carbon nanotubes at 40 cm bed thickness at three flow rates 14 lpm, 19 lpm and 29 lpm for 2 mm, 4 mm and 6 mm glass beads without the effects of electrostatic forces. All the results show that the filter efficiencies decrease with increasing particle size. The filtration efficiency for 2 mm glass beads is higher than that for 4 mm glass beads. However, Figure 4-14 (a) shows that for particles above 50nm and Figure 4-14 (b) and Figure 4-14 (c) show that for particles above 25nm, the filtration efficiency for 6 mm is higher than that for 4 mm glass beads. For 6 mm glass beads, the space among collectors is large, and the bed thickness is high, which leads to a long resistance time for carbon nanotubes. The CNTs in the fluid may aggregate and become bundles. Then, another mechanism, straining or sieving could become significant, which increases the filtration efficiency.

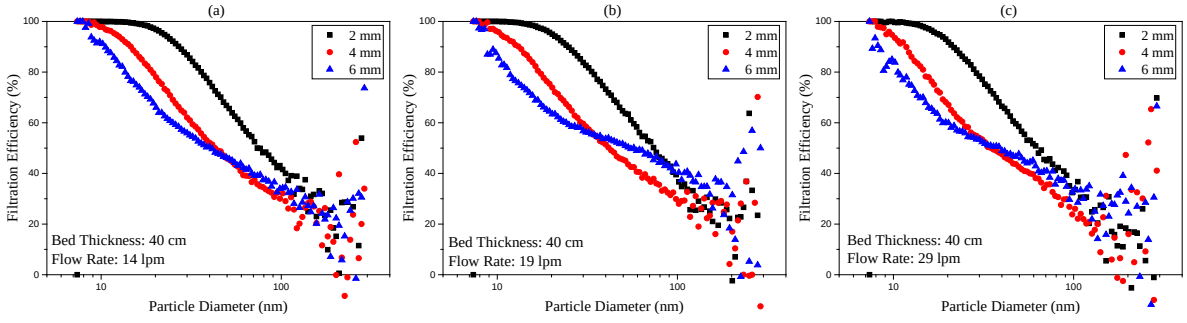

Figure 4-14 Filtration efficiency of nanotubes at 40 cm bed thickness at different flow rates for three glass beads

4.4 Summary

Experiments were carried out to measure the granular filtration efficiencies of carbon nanotubes without the effects of electrostatic forces. The results showed that the overall granular bed filtration efficiencies decreased with increasing particle size, which indicated that the dominant mechanism is Brownian diffusion. The flow rates had an adverse effect on the filtration efficiency. As the bed thickness increased, the filtration efficiency increased as well. Moreover, the fine granule media diameter was a favorable factor for increasing filtration efficiency.

The experiment results could be used to compare with the values obtained by models for prediction of granular filtration efficiency, which will be introduced in the next chapter.

Chapter 5
Modeling of Granular Filtration

5.1 Overview

In this chapter, some assumptions were applied to simplify the complicated granular filtration process and make the modeling of granular filtration feasible. And then the flow field model was chosen, and the expression for single collector efficiency was determined. By applying the single collector efficiency in the overall bed filter model, the overall granular filtration efficiency could be obtained.

The experimental results from Chapter 4 were compared with the values calculated by four theoretical models. These four models have the same trend as the experimental results. The filtration efficiencies are inversely proportional to the size of the particles. For 2 mm glass beads, the UBE model has a good agreement with the experiment results. Concerning 4 mm glass beads, Tardos's model fits the experiment results better. With respect to 6 mm glass beads, at 10 cm bed thickness, Tardos's model fits the experimental results very well. At 20 cm and 40 cm bed thickness, Tardor's model underestimates the filtration efficiencies, and the divergence is getting more prominent as the bed thickness increased.

5.2 Assumptions

The process of the granular filtration is very complicated. The filtration efficiency depends on many parameters, including bed filter characteristics, such as bed thickness, bed geometry and bed porosity; superficial velocity and flow field; the characteristics of granular media, such as the geometry, size, size distribution and surface chemistry of the collectors; and the characteristics of particles, such as shape, size, size distribution, temperature, viscosity and solution chemistry of the suspending particles. Since so many factors affect filtration efficiency, some assumptions have been made to simplify the conditions to build the modeling.

1. The granular collectors are spheres with identical size and homogeneously distribution;
2. The presence of deposited particles on the surface of granular collectors will not affect the filtration efficiency;
3. There is no re-entrainment effect for deposited particles.

5.3 Overall filtration efficiency of granular bed

In this section, a model of granular bed filtration will be developed based on the knowledge of basic filtration mechanisms.

As the granular bed is randomly packed, the realistic flow field can be described as chaotic and complex. A simplified flow field model should be used to make the prediction feasible. Since spherical glass beads were used as granular media in this study, the spherical model was selected as the flow field model. Among the three spherical models introduced in Chapter 2, Happel's model [64] and Kuwabara's model [65] are better than the isolated-sphere model. The isolated-sphere model views the collector totally independent regardless of the interaction between collectors, which is in disagreement with the reality of the filtration process. Happel's model [64] is the same as Kuwabara's model [65] in conception and formulation, and only the boundary conditions applied are different. Therefore, the differences between these two models are minimal. In this study, Happel's model was used to calculate the filtration efficiency.

As mentioned in section 2.5.1, there are five main mechanisms responsible for the collision, inertial impaction, interception, sedimentation, Brownian diffusion and electrostatic forces. As inertial impaction mechanism is important for particles above 1μm and the mass of the nanosized particles are very small, the effects of the inertial impaction and sedimentation on filtration of nanosized particles can be negligible. The effects of the electrostatic forces are significant for nanoparticle filtration as shown by the experiment results. However, it is difficult to predict the charges on particles and collectors. Only filtration efficiency for the neutralized particles was calculated in this study. Therefore, the mechanisms attributed to the single collector collision efficiency are interception and Brownian diffusion. It can be expressed as applying Eqn (2.58)

$$\eta_c = 1 - [1 - (\eta_c)_I][1 - (\eta_c)_{BM}] \tag{5.1}$$

The differential mobility analyzer (DMA) was used in this study to measure the size distribution of carbon nanotubes. For a spherical particle, the electrical mobility diameter is equivalent to its geometric diameter. For non-spherical particles, the measured electrical mobility diameter is that for a sphere of equivalent mobility.

Spherical or spherical-like particles may have only one characteristic dimension. However, elongated aerosol particles including carbon nanotubes have two characteristic dimensions, the diameter and length. Both of them may affect the carbon nanotubes behaviors in the filtration process.

However, it is difficult to determine the diameter and length of each nanotube. Only electrical diameter is measurable in the experiments.

Kim et al. [105] have developed a theoretical model which enabled to express the lengths of monodisperse carbon nanotubes as a function of the mobility diameter of the nanotubes.

Bahk et al. [46] developed another model to describe the relationship between the geometrical length and electrical mobility diameter of cylinder shaped particles. They consider two cases, random orientation and total aligned orientation for the free molecular and transition regimes. For the random orientation in the free molecular regime, the geometrical length of a carbon nanotube can be expressed as

$$l_{cnt} = \frac{A_{cnt}\lambda d_p}{d_{cnt}C_s} \tag{5.2}$$

where

$$A_{cnt} = 2\left(\frac{1}{f} + \frac{2}{\frac{\pi-2}{4}+2}\right) \tag{5.3}$$

where f is the momentum accommodation coefficient and equal to 0.9.

For the total alignment

$$l_{cnt} = \frac{6\lambda d_p}{f d_{cnt}C_s} \tag{5.4}$$

However, we still need to know either the diameter or geometrical length of carbon nanotubes to calculate the other one, which is required for calculating the efficiency due to interception and Brownian diffusion. Therefore, we can only use the measured electrical mobility diameter as the parameter in the calculation.

$(\eta_c)_I$ is determined by Eqn (2.38) and $(\eta_c)_{BM}$ is determined by Eqn (2.54).

Since there was no thermal rebound occurrence in experiment results, the adhesion efficiency was assumed to be unity. Thus, the single collector efficiency is the same as the single collector collision efficiency, as

$$\eta_s = \eta_c \tag{5.5}$$

For the overall granular bed filtration, Yao's model [50], Tardos's model [51] and Boulaud's model [88] were used to calculate the filtration efficiency. The formulas given in Chapter 2 are as follows

$$\eta_{filter} = 1 - exp\left[-\frac{3}{2}(1-\varepsilon)\eta_s\left(\frac{L}{d_g}\right)\right] \quad (2.61)$$

$$\eta_{filter} = 1 - \exp\left[-\frac{3}{2}\frac{(1-\varepsilon)}{\varepsilon}\eta_s\left(\frac{L}{d_g}\right)\right] \quad (2.62)$$

$$\eta_{filter} = 1 - exp\left[-\frac{3}{2}\varepsilon\eta_s\left(\frac{L}{d_g}\right)\right] \quad (2.63)$$

Bed porosity has a significant effect on filtration efficiency. It not only affects the flow field and the single collector efficiency consequently but also has an important effect on the correlation between the single collector efficiency and the overall filtration efficiency. The bed porosity is defined as the free volume fraction of the fixed granular bed. Pushnov [106] proposed a formula for engineering evaluation of the bed porosity, which was

$$\varepsilon = \frac{A}{\left({}^{D_f}/_{d_g}\right)^n} + B \qquad \text{for } {}^{D_f}/_{d_g} > 2 \text{ and } L > 20d_g \quad (5.6)$$

$$\varepsilon = 12.6\left({}^{D_f}/_{d_g}\right)^{6.1} exp\left(-3.6\,{}^{D_f}/_{d_g}\right) \qquad \text{for } {}^{D_f}/_{d_g} < 2.4 \quad (5.7)$$

where D_f is the diameter of the granular bed; A, B and n are constants depend on the shape of the granules which are given in Table 5-1.

Table 5-1 The coefficients for calculation of the bed porosity [106]

Shape of Granules	Coefficients		
	A	B	n
Spherical	1.0	0.375	2

In the UBE model, the entire granular filter can be viewed as a collection of UBE which consists of a number of collectors. The overall filtration efficiency can be obtained by calculating the efficiency of each UBE which is determined by the single collector efficiency. As mentioned above, the single collector efficiency is equal to the single collector collision efficiency, which is given by Eqn (5.5). Since Happel's model was used in this study, the relationship between the single collector efficiency and the filtration efficiency of UBE was given by Eqn (2.25). The overall filtration efficiency is given by equation (2.66), which is

$$\eta_{filter} = 1 - \prod_{i=1}^{N}(1 - e_i) \quad (2.66)$$

And N is given by Eqn (2.67).

For the filtration of carbon nanotubes, the granular bed is straight, and the flow is downward. Therefore, the bed thickness is the bed height. With respect to the filtration of the nanosized NaCl particles, there is a tube which introduces the particles into the filter bed. The flow goes down first, and then it turns to go upward. Therefore, the active bed thickness should be divided into two parts, the bed height above the contact level and the bed thickness which particles go through below the contact level. As the bed thickness below the contact level cannot be measured in the experiments, the active bed thickness must be made arbitrarily to predict the filtration efficiency. As a result, only the experimental results of carbon nanotubes filtration were compared with the filtration efficiencies predicted by the theoretical models.

5.4 Comparisons between the models and the experimental results for filtration of carbon nanotubes

Figure 5-1 shows the comparisons of the experimental results with theoretical models for 2 mm glass beads at three flow rates at three bed thicknesses. The four models have the same trend as experimental results. The filtration efficiencies decrease with increasing particle size. Among the four theoretical models, Tardos's model always has the highest filtration efficiencies, and Boulaud's model has the lowest. The filtration efficiency of the UBE model is higher than that of Yao's model. The UBE model has a good agreement with the experiment results. As the single collector efficiency is the same, the differences between the models are due to the method used to develop the single collector efficiency to the whole bed filter. The UBE model divides the total granular bed filter into layers which are decided by the single collector efficiency. Other models calculate the summation of all single collection effect by direct integration, which may result in the accumulation of calculating errors.

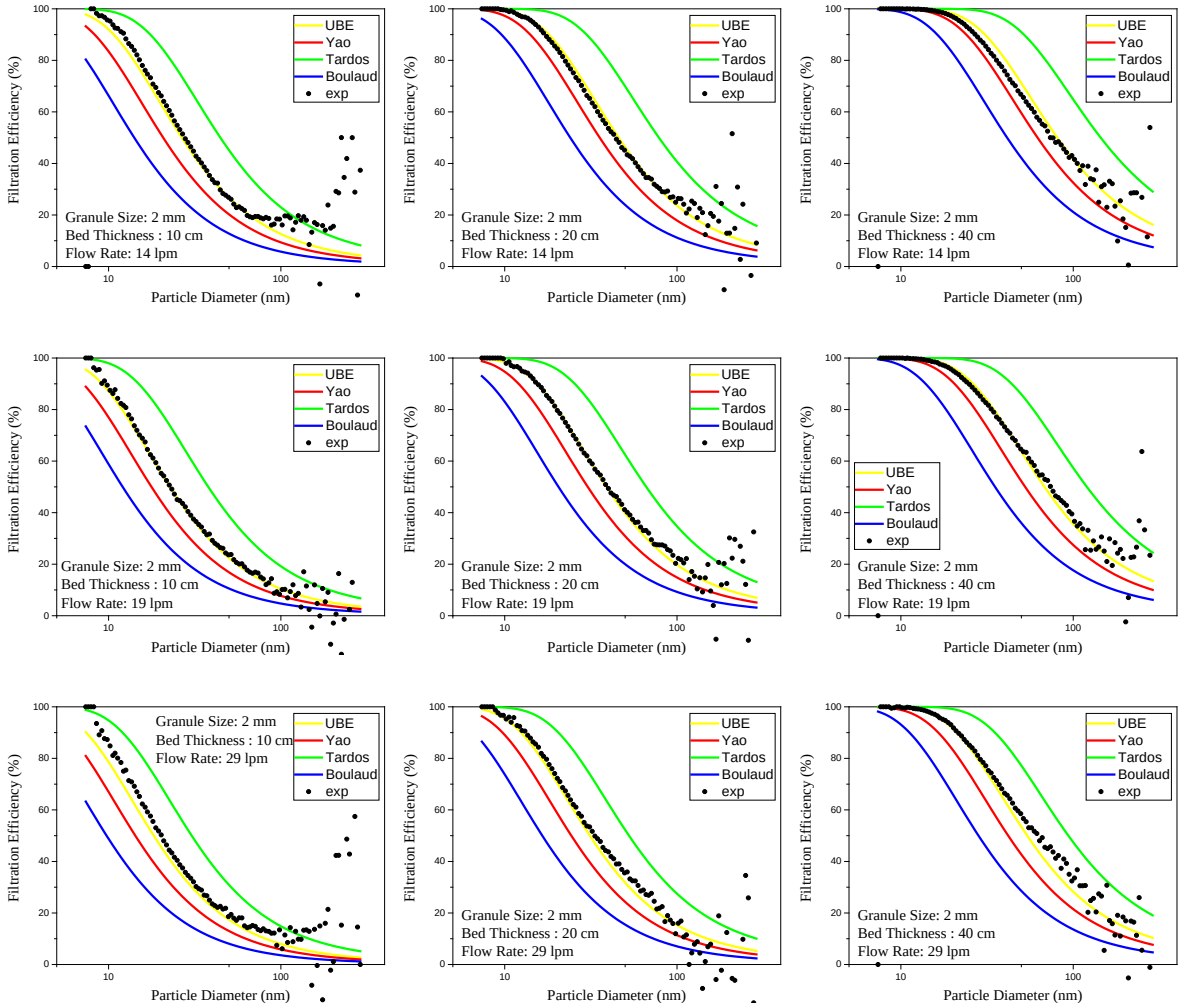

Figure 5-1 Comparisons of the experimental results with theoretical models for 2 mm glass beads at three flow rates at three bed thicknesses

Figure 5-2 shows the comparisons of the experimental results with theoretical models for 4 mm glass beads at three flow rates at three bed thicknesses. The trends of the four theoretical models and the relationships among them are the same as what is shown in Figure 5-1. However, the UBE model does not fit the experimental results very well, and Tardos's model is better. In most cases, the filtration efficiency lines calculated by Tardos' model cross the experimental results lines. It overestimates the filtration efficiency for small particles and underestimates the filtration efficiency for larger particles. For the other three models, they all underestimate the filtration efficiency. As the diameter of the glass beads increases to 4mm, the bed porosity changes, which affects most factors influencing the filtration efficiency, such as the flow field, the single collector efficiency and the

overall filtration efficiency. Since the bed is random packed and the bed porosity may be not true for the reality, theoretical models depending on the bed porosity may not predict the filtration efficiency very well. That may be the reason why the models do not fit the experimental results very well.

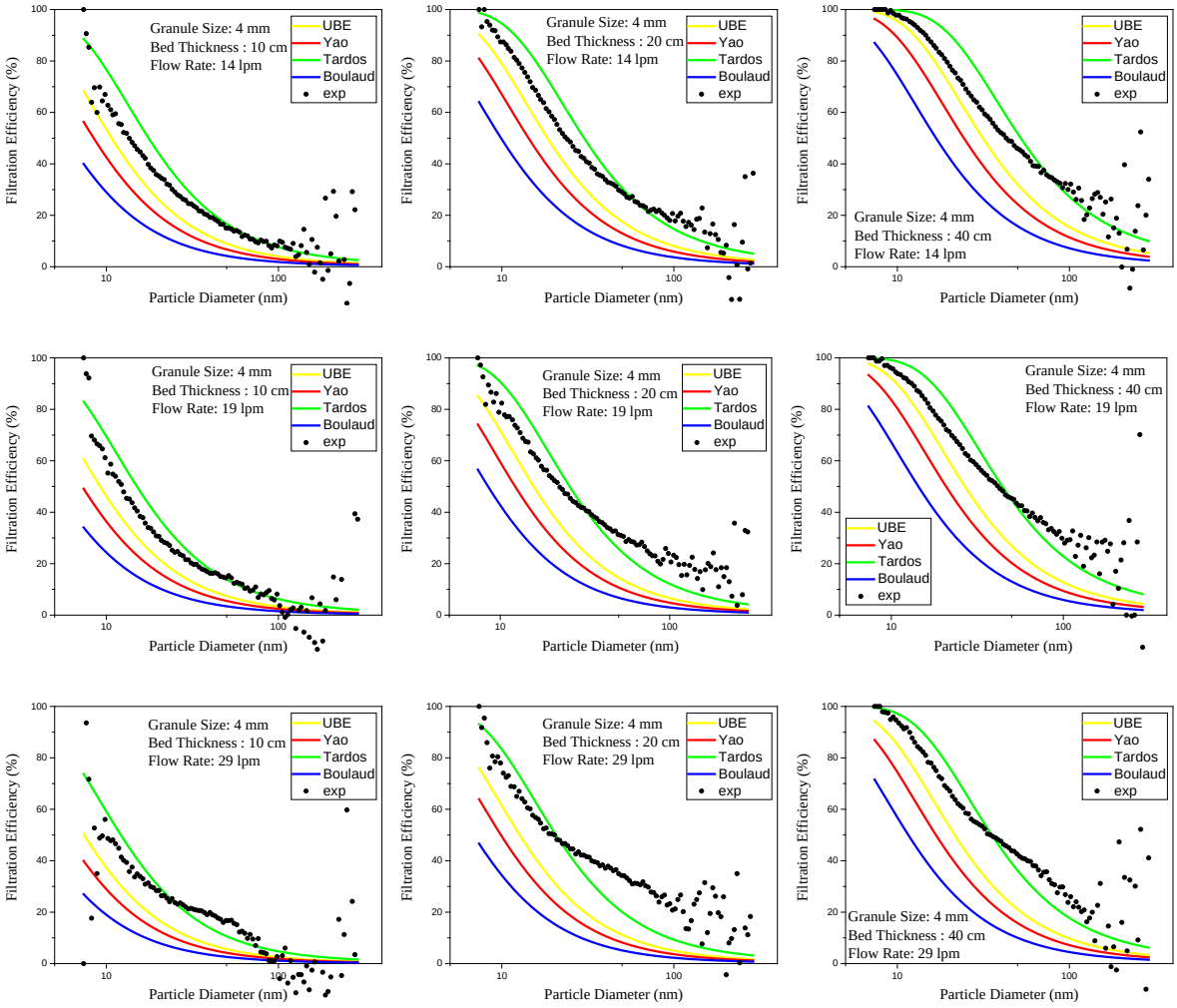

Figure 5-2 Comparisons of the experimental results with theoretical models for 4 mm glass beads at three flow rates at three bed thicknesses

Figure 5-3 shows the comparisons of the experimental results with theoretical models for 6 mm glass beads at three flow rates at three bed thicknesses. The trends of the four theoretical models and the relationships among them are the same as what is shown in Figure 5-2. At 10 cm bed thickness, Tardos's model fits the experimental results better than the other three models do. At 20 cm and 40 cm bed thickness, Tardor's model underestimates the filtration efficiencies, and the divergence is getting bigger as the bed thickness increased. The increased bed thickness expends the error in the

calculation of the single collector efficiency and the summation of the single filter element. As mentioned in Chapter 4, there is more space in the filter bed for larger granular collectors, especially for high bed thickness. The CNTs may aggregate and become bundles. In that case, the effect of straining or sieving may become significant for granular filtration. However, this mechanism is not included in the calculation of the single collector efficiency. That is maybe another reason why all models underestimate the filtration efficiency.

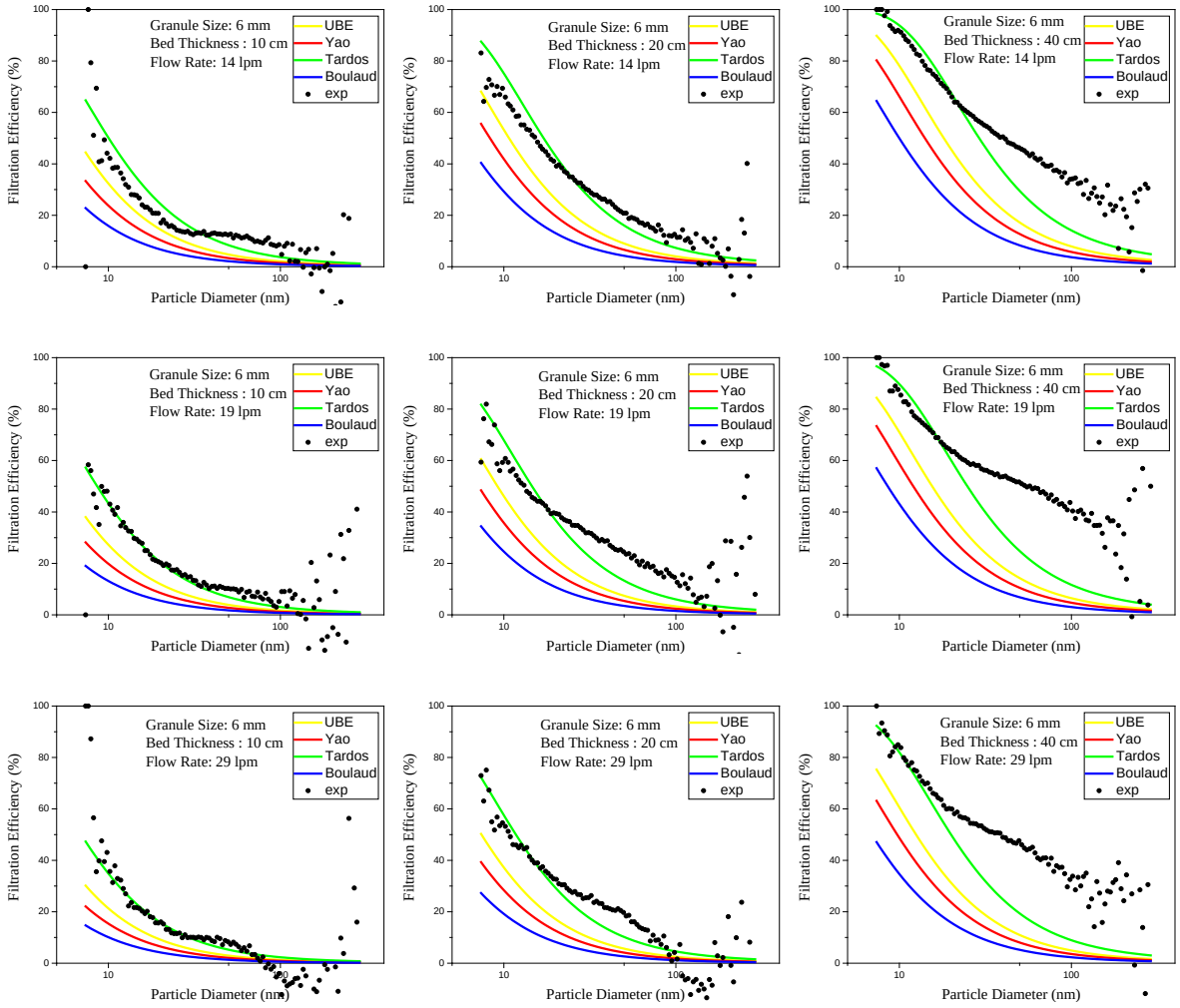

Figure 5-3 Comparisons of the experimental results with theoretical models for 6 mm glass beads at three flow rates at three bed thicknesses

5.5 Summary

In this chapter, the theoretical models were developed to predict the efficiency of granular filtration. The experimental results were compared with the values calculated by four different models. The four models have the same trend as the experimental results. The filtration efficiencies decrease with increasing particle size. Among the four theoretical models, Tardos's model always has the highest filtration efficiencies, and Boulaud's model has the lowest. The filtration efficiencies calculated by the UBE model is higher than that by Yao's model. For 2 mm glass beads, the UBE model has a good agreement with the experimental results. With respect to 4 mm glass beads, Tardos's model fits the experimental results better. In most case, the filtration efficiency lines calculated by Tardos' model cross the experimental result lines. It overestimates the filtration efficiency for small particles and underestimates the filtration efficiency for large particles. By 6 mm glass beads, at 10 cm bed thickness, Tardos's model fitted the experimental results very well. At 20 cm and 40 cm bed thickness, Tardor's model underestimates the filtration efficiencies, and the divergence is getting more significant as the bed thickness increases.

Chapter 6
Conclusions and Future Work

6.1 Conclusions

Experiments were carried out to study the effects of the electrostatic forces on filtration efficiency of nanosized NaCl particles and the granular filtration of carbon nanotubes.

For naturally charged NaCl particles, the electrostatic forces can significantly increase the overall filtration efficiency of large particles and reduce the filtration efficiency of small particles. The polarities on small particles and large particles are different, and the polarity on the granular media is specific. Therefore, the electrostatic forces are attractive and repulsive for large particles and small particles, respectively. The experimental results show that a higher flow rate leads to higher filtration efficiency only due to electrostatic forces. Moreover, low bed thickness has a positive effect on the filtration efficiency only due to electrostatic forces. For 2 mm granular media diameter, the filtration efficiencies only due to electrostatic forces increase with increasing particle size. For 4 mm and 6 mm glass beads, the filtration efficiencies only due to electrostatic forces have an "n" shape. Filtration efficiencies only due to electrostatic forces increase with increasing particle size and decrease with increasing particle size after the efficiencies reach the summit.

For carbon nanotubes, the experimental results show that the filtration efficiency follows the conventional theory. The overall granular bed filtration efficiency decreases with increasing particle size, which indicates that the dominant mechanism is Brownian diffusion. The high flow rates have an adverse effect on the filtration efficiency. As the bed thickness increases, the filtration efficiency increases. Moreover, the fine granule media diameter is a favorable factor to improve filtration efficiency. Some results do not agree with the conclusions mentioned above. The reason may be the geometry of the granular bed, which leads to complex flow field and filtration process for the particles.

Four theoretical models have been compared with the experimental results of granular filtration of carbon nanotubes. The four models have the same trend as the experimental results. The filtration efficiency decreases with increasing particle size. Among the four theoretical models, Tardos's model always has the highest filtration efficiency, and Boulaud's model has the lowest. The filtration efficiencies calculated by the UBE model are higher than that by Yao's model. For 2 mm glass beads, the UBE model has a good agreement with the experimental results. Concerning 4 mm glass beads,

Tardos's model fits the experimental results better. In most cases, the filtration efficiency lines calculated by Tardos' model cross the experimental lines. Tardos' model overestimates the filtration efficiency for small particles and underestimates the filtration efficiency for large particles. With respect to 6 mm glass beads, at 10 cm bed thickness, Tardos's model fits the experimental results very well. At 20 cm and 40 cm bed thickness, Tardor's model underestimates the filtration efficiencies, and the divergence is getting more significant as the bed thickness increases.

6.2 Future work

More experiments should be carried out to study why the filtration efficiency only due to the electrostatic forces has an "n" shape.

The charges on the particles and granular media could be measured and quantified in order to predict the filtration efficiency with the electrostatic forces using theoretical models.

As carbon nanotubes have a cylindrical shape, the shape factor should be considered to study the filtration process. And knowing the diameters and the lengths of carbon nanotubes is helpful to obtain more accurate prediction of filtration efficiency.

References

1. EPA, *Particulate Matter (PM) Pollution*. 2017 [cited 2017; Available from: https://www.epa.gov/pm-pollution.
2. EPA. *Criteria Air Pollutants*. 2017 [cited 2017 Jan 3]; Available from: https://www.epa.gov/criteria-air-pollutants.
3. Ministry of the Environment, Conservation and Parks of Ontario. *Information: About Air Quality*. 2018 [cited 2018 June]; Available from: http://www.airqualityontario.com/science/index.php#monitor.
4. Hinds, W.C., *Aerosol Technology: Properties, Behaviour, and Measurement of Airborne Particles.* Journal of Aerosol Science, 1999. **31**(9): p. 1121–1122.
5. Iijima, S., *Helical microtubules of graphitic carbon.* Nature, 1991. **354**(6348): p. 56-58.
6. Baughman, R.H., A.A. Zakhidov, and W.A. de Heer, *Carbon nanotubes--the route toward applications.* Science, 2002. **297**(5582): p. 787-792.
7. Frank, E.A., et al., *Carbon nanotube and asbestos exposures induce overlapping but distinct profiles of lung pathology in non-swiss Albino CF-1 mice.* Toxicologic Pathology, 2016. **44**(2): p. 211.
8. Bonner, J.C., et al., *Interlaboratory Evaluation of Rodent Pulmonary Responses to Engineered Nanomaterials: The NIEHS Nano GO Consortium.* Environmental Health Perspectives, 2013. **121**(6): p. 676-682.
9. Mercer, R.R., et al., *Pulmonary fibrotic response to aspiration of multi-walled carbon nanotubes.* Particle & Fibre Toxicology, 2011. **8**(1): p. 21.
10. Lam, C.W., et al., *Pulmonary Toxicity of Single-Wall Carbon Nanotubes in Mice 7 and 90 Days After Intratracheal Instillation.* Toxicological Sciences, 2004. **77**(1): p. 126-134.
11. Sargent, L.M., et al., *Promotion of lung adenocarcinoma following inhalation exposure to multi-walled carbon nanotubes.* Particle & Fibre Toxicology, 2014. **11**(1): p. 3.
12. Park, S.H., et al., *Wet scrubbing of polydisperse aerosols by freely falling droplets.* Journal of Aerosol Science, 2005. **36**(12): p. 1444-1458.
13. Golshahi, L., J. Abedi, and Z. Tan, *Granular filtration for airborne particles: Correlation between experiments and models.* Canadian Journal of Chemical Engineering, 2009. **87**(5): p. 726–731.
14. Menegolla, H.B., et al., *Filtration of dust in an intermittent moving granular bed filter: Performance and modeling.* Separation & Purification Technology, 2014. **133**(36): p. 108-119.
15. El-Hedok, I.A., L. Whitmer, and R.C. Brown, *The influence of granular flow rate on the performance of a moving bed granular filter.* Powder Technology, 2011. **214**(1): p. 69-76.
16. Peukert, W. and C. Wadenpohl, *Industrial separation of fine particles with difficult dust properties.* Powder Technology, 2001. **118**(1–2): p. 136-148.
17. Saxena, S.C., R.F. Henry, and W.F. Podolski, *Particulate removal from high-temperature, high-pressure combustion gases.* Progress in Energy & Combustion Science, 1985. **11**(3): p. 193-251.
18. Xiao, G., et al., *Granular bed filter: A promising technology for hot gas clean-up.* Powder Technology, 2013. **244**(4): p. 93-99.
19. Chi, T. and B.V. Ramarao, *Granular Filtration of Aerosols and Hydrosols (Second Edition).* 2007.
20. Oswaldo B. Duarte Fo., et al., *Filtration of Electrified Solid Particles.* Industrial & Engineering Chemistry Research, 2000. **39**(10): p. 3884-3895.

21. Shapiro, M., G. Laufer, and C. Gutfinger, *Electrostatically Enhanced Granular Bed Filters.* Aerosol Science and Technology, 1986. **5**(1): p. 39-54.
22. Mauter, M.S. and M. Elimelech, *Environmental applications of carbon-based nanomaterials.* Environmental Science & Technology, 2008. **42**(16): p. 5843.
23. Hu, Y., O.A. Shenderova, and D.W. Brenner, *Carbon Nanostructures: Morphologies and Properties.* Journal of Computational & Theoretical Nanoscience, 2007. **4**(2): p. 199-221.
24. Wang, J., S.C. Kim, and D.Y.H. Pui, *Measurement of multi-wall carbon nanotube penetration through a screen filter and single-fiber analysis.* Journal of Nanoparticle Research, 2011. **13**(10): p. 4565-4573.
25. Wang, J., S.C. Kim, and D.Y.H. Pui, *Carbon Nanotube Penetration through a Screen Filter: Numerical Modeling and Comparison with Experiments.* Aerosol Science & Technology, 2011. **45**(3): p. 443-452.
26. Endo, M., M.S. Strano, and P.M. Ajayan, *Potential Applications of Carbon Nanotubes.* Topics in Applied Physics, 2007. **111**(5): p. 13-61.
27. Mckinney, W., B. Chen, and D. Frazer, *Computer controlled multi-walled carbon nanotube inhalation exposure system.* Inhalation Toxicology, 2009. **21**(12): p. 1053-61.
28. Chakravarty, P., et al., *Thermal ablation of tumor cells with antibody-functionalized single-walled carbon nanotubes.* Proceedings of the National Academy of Sciences of the United States of America, 2008. **105**(25): p. 8697.
29. Poland, C.A., et al., *Carbon nanotubes introduced into the abdominal cavity of mice show asbestos-like pathogenicity in a pilot study.* Nature Nanotechnology, 2008. **3**(7): p. 423-8.
30. Murphy, F.A., et al., *Length-dependent pleural inflammation and parietal pleural responses after deposition of carbon nanotubes in the pulmonary airspaces of mice.* Nanotoxicology, 2013. **7**(6): p. 1157-67.
31. Mercer, R.R., et al., *Distribution and persistence of pleural penetrations by multi-walled carbon nanotubes.* Particle & Fibre Toxicology, 2010. **7**(1): p. 28.
32. Chen, B.T., *Acute pulmonary dose-responses to inhaled multi-walled carbon nanotubes.* Nanotoxicology, 2013. **7**(7): p. 1179.
33. Mitchell, L., et al., *Pulmonary and systemic immune response to inhaled multiwalled carbon nanotubes.* Toxicological Sciences An Official Journal of the Society of Toxicology, 2007. **100**(1): p. 203-214.
34. Porter, D.W., et al., *Mouse pulmonary dose- and time course-responses induced by exposure to multi-walled carbon nanotubes.* Toxicology, 2010. **269**(2-3): p. 136.
35. Wick, P., et al., *The degree and kind of agglomeration affect carbon nanotube cytotoxicity.* Toxicology Letters, 2007. **168**(2): p. 121.
36. Sayes, C.M., et al., *Functionalization density dependence of single-walled carbon nanotubes cytotoxicity in vitro.* Toxicology Letters, 2006. **161**(2): p. 135-142.
37. Shvedova, A.A., et al., *Inhalation vs. aspiration of single-walled carbon nanotubes in C57BL/6 mice: inflammation, fibrosis, oxidative stress, and mutagenesis.* Am J Physiol Lung Cell Mol Physiol, 2008. **295**(4): p. L552.
38. Muller, J., et al., *Structural Defects Play a Major Role in the Acute Lung Toxicity of Multiwall Carbon Nanotubes: Toxicological Aspects.* Chemical Research in Toxicology, 2008. **21**(9): p. 1698.
39. Chen, S.C., et al., *Carbon Nanotube Penetration Through Fiberglass and Electret Respirator Filter and Nuclepore Filter Media: Experiments and Models.* Aerosol Science & Technology, 2014. **48**(10): p. 997-1008.

40. Vo, E. and Z. Zhuang, *Development of a new test system to determine penetration of multi-walled carbon nanotubes through filtering facepiece respirators.* Journal of Aerosol Science, 2013. **61**(3): p. 50-59.
41. Wang, J., *Effects of Particle Size and Morphology on Filtration of Airborne Nanoparticles.* KONA Powder and Particle Journal, 2013. **30**: p. 256-266.
42. Seto, T., et al., *Filtration of Multi-Walled Carbon Nanotube Aerosol by Fibrous Filters.* Aerosol Science and Technology, 2010. **44**(9): p. 734-740.
43. Liu, X., et al., *Mobility of Multiwalled Carbon Nanotubes in Porous Media.* Environmental Science & Technology, 2009. **43**(21): p. 8153-8158.
44. Jaisi, D. and M. Elimelech, *Single-Walled Carbon Nanotubes Exhibit Limited Transport in Soil Columns*. Vol. 43. 2009. 9161-6.
45. Jaisi, D., et al., *Transport of Single-Walled Carbon Nanotubes in Porous Media: Filtration Mechanisms and Reversibility*. Vol. 42. 2008. 8317-23.
46. Bahk, Y.K., J. Buha, and J. Wang, *Determination of Geometrical Length of Airborne Carbon Nanotubes by Electron Microscopy, Model Calculation, and Filtration Method.* Aerosol Science and Technology, 2013. **47**(7): p. 776-784.
47. Lall, A.A. and S.K. Friedlander, *On-line measurement of ultrafine aggregate surface area and volume distributions by electrical mobility analysis: I. Theoretical analysis.* Journal of Aerosol Science, 2006. **37**(3): p. 260-271.
48. Li, M., G.W. Mulholland, and M.R. Zachariah, *The Effect of Orientation on the Mobility and Dynamic Shape Factor of Charged Axially Symmetric Particles in an Electric Field.* Aerosol Science & Technology, 2012. **46**(9): p. 1035-1044.
49. Mattison, N.T., et al., *Impact of Porous Media Grain Size on the Transport of Multi-walled Carbon Nanotubes.* Environmental Science & Technology, 2011. **45**(22): p. 9765-9775.
50. Yao, K.M., M.T. Habibian, and C.R. O'Melia, *Water and waste water filtration. Concepts and applications.* Environmental Science & Technology, 1971. **5**(11).
51. G.Tardos, C.G., N.Abuaf, *Deposition of Dust Particles in a Fluidized Bed Filter.* Israel J. Tech, 1974. **12**: p. 184-190.
52. Payatakes, A.C., T. Chi, and R.M. Turian, *A new model for granular porous media: Part I. Model formulation.* Aiche Journal, 1973. **19**(1): p. 58-67.
53. Tardos, G.I., N. Abuaf, and C. Gutfinger, *Dust Deposition in Granular Bed Filters: Theories and Experiments.* Journal of the Air & Waste Management Association, 1978. **28**(4): p. 354-363.
54. Chi, T. and A.C. Payatakes, *Advances in deep bed filtration.* Aiche Journal, 1979. **25**(5): p. 737–759.
55. Scheidegger, A.E., *The Physics of Flow Through Porous Media*. 1957: Macmillan.
56. Rajagopalan, R. and C. Tien, *The Theory of Deep Bed Filtration* Progress in Filtration and Separation, 1979. **1**.
57. Jackson, S. and S. Calvert, *Entrained particle collection in packed beds.* Aiche Journal, 1966. **12**(6): p. 1075-1078.
58. Petersen, E.E., *Diffusion in a pore of varying cross section.* Aiche Journal, 1958. **4**(3): p. 343-345.
59. Gal, E., G. Tardos, and R. Pfeffer, *A study of inertial effects in granular bed filtration.* Aiche Journal, 1985. **31**(7): p. 1093-1104.
60. Payatakes, A.C., T. Chi, and R.M. Turian, *A new model for granular porous media: Part II. Numerical solution of steady state incompressible Newtonian flow through periodically constricted tubes.* Aiche Journal, 1973. **19**(1): p. 67-76.

61. Neira, M.A. and A.C. Payatakes, *Collocation solution of creeping newtonian flow through periodically constricted tubes with piecewise continuous wall profile.* Aiche Journal, 1978. **24**(1): p. 43-54.
62. Fedkiw, P. and J. Newman, *Entrance region (Lévêquelike) mass transfer coefficients in packed bed reactors.* Aiche Journal, 1979. **25**(6): p. 1077-1080.
63. Venkatesan, M. and R. Rajagopalan, *A hyperboloidal constricted tube model of porous media.* Aiche Journal, 1980. **26**(4): p. 694-698.
64. Happel, J., *Viscous flow in multiparticle systems: Slow motion of fluids relative to beds of spherical particles.* Aiche Journal, 1958. **4**(2): p. 197-201.
65. Kuwabara, S., *The Forces experienced by Randomly Distributed Parallel Circular Cylinders or Spheres in a Viscous Flow at Small Reynolds Numbers.* Journal of the Physical Society of Japan, 1959. **14**(4): p. 527.
66. Chi, T. and H. Brenner, *Granular Filtration of Aerosols and Hydrosols.* 2007.
67. Ives, K.J., *Rapid filtration.* Water Research, 1970. **4**(3): p. 201-223.
68. Cunningham, E., *On the Velocity of Steady Fall of Spherical Particles through Fluid Medium.* Proceedings of the Royal Society of London. Series A, 1910. **83**(563): p. 357-365.
69. Davies, C.N., *Definitive equations for the fluid resistance of spheres.* Proceedings of the Physical Society, 1945. **57**(4): p. 259.
70. Beizaie, M., *Deposition of Particles on a Single Collector*. 1977, Syracuse University.
71. Rajagopalan, R. and T. Chi, *Trajectory analysis of deep‐bed filtration with the sphere‐in‐cell porous media model.* Aiche Journal, 1976. **22**(3): p. 523-533.
72. Ruckenstein, E., *On mass transfer in the continuous phase from spherical bubbles or drops.* Chem. Engng Sci, 1964. **19**: p. 131.
73. Ruckenstein, E., *On mass transfer in the continuous phase from spherical bubbles or drops.* Chemical Engineering Science, 1964. **19**(2): p. 131-146.
74. Bruckenstein, S., *Physicochemical Hydrodynamics*. 1962: Prentice-Hall. 75-75.
75. Tardos, G., et al., *Filtration of airborne dust in a triboelectrically charged fluidized bed.* Industrial & Engineering Chemistry Fundamentals, 1983. **22**(4): p. 445-453.
76. Kraemer, H.F. and H.F. Johnstone, *Collection of Aerosol Particles in Presence of Electrostatic Fields.* Industrial & Engineering Chemistry, 1955. **47**(12): p. 2426-2434.
77. Wang, H.C. and G. Kasper, *Filtration efficiency of nanometer-size aerosol particles.* Journal of Aerosol Science, 1991. **22**(1): p. 31-41.
78. Alonso, M., et al., *Penetration of Nanometer-Sized Aerosol Particles Through Wire Screen and Laminar Flow Tube.* Aerosol Science and Technology, 1997. **27**(4): p. 471-480.
79. Heim, M., et al., *Filtration Efficiency of Aerosol Particles Below 20 Nanometers.* Aerosol Science and Technology, 2005. **39**(8): p. 782-789.
80. Kim, S.C., M.S. Harrington, and D.Y.H. Pui, *Experimental study of nanoparticles penetration through commercial filter media*. 2006: Springer Netherlands. 117-125.
81. Japuntich, D.A., et al., *A comparison of two nano-sized particle air filtration tests in the diameter range of 10 to 400 nanometers.* Journal of Nanoparticle Research, 2006. **9**(1): p. 93-107.
82. Huang, S.-H., et al., *Penetration of 4.5 nm to aerosol particles through fibrous filters.* Journal of Aerosol Science, 2007. **38**(7): p. 719-727.
83. Shin, W.G., et al., *Experimental study of filtration efficiency of nanoparticles below 20 nm at elevated temperatures.* Journal of Aerosol Science, 2008. **39**(6): p. 488-499.

84. Golanski, L., et al., *Experimental evaluation of personal protection devices against graphite nanoaerosols: fibrous filter media, masks, protective clothing, and gloves.* Human & Experimental Toxicology, 2009. **28**(6-7): p. 353-359.
85. Heim, M., M. Attoui, and G. Kasper, *The efficiency of diffusional particle collection onto wire grids in the mobility equivalent size range of 1.2–8 nm.* Journal of Aerosol Science, 2010. **41**(2): p. 207-222.
86. Bałazy, A., A. Podgórski, and L. Gradoń, *Filtration of nanosized aerosol particles in fibrous filters. I – experimental results.* Journal of Aerosol Science, 2004. **35**: p. 967-980.
87. Shapiro, M., C. Gutfinger, and G. Laufer, *Electrostatic mechanisms of aerosol collection by granular filters: A review.* Journal of Aerosol Science, 1988. **19**(6): p. 651-677.
88. Boulaud, D., *Use of granular beds in the inertial impaction regime for aerosol size distribution measurement.* Journal of Aerosol Science, 1991. **22**(3): p. 273-287.
89. Reischl, G.P., H.G. Scheibel, and J. Porstendörfer, *The bipolar charging of aerosols: Experimental results in the size range below 20-nm particle diameter.* Journal of Colloid and Interface Science, 1983. **91**(1): p. 272-275.
90. Kousaka, Y., et al., *Bipolar Charging of Ultrafine Aerosol Particles.* Aerosol Science and Technology, 1983. **2**(4): p. 421 - 427.
91. Fuchs, N.A., *On the stationary charge distribution on aerosol particles in a bipolar ionic atmosphere.* Pure and Applied Geophysics, 1963. **56**(1): p. 185-193.
92. Wiedensohler, A., *An approximation of the bipolar charge distribution for particles in the submicron size range.* Journal of Aerosol Science, 1988. **19**(3): p. 387-389.
93. Forsyth, B., B.Y.H. Liu, and F.J. Romay, *Particle Charge Distribution Measurement for Commonly Generated Laboratory Aerosols.* Aerosol Science and Technology, 1998. **28**(6): p. 489 - 501.
94. Tardos, G.I., C. Gutfinger, and R. Pfeffer, *Triboelectric Effects in Filtration of Small Dust Particles in a Granular Bed.* Industrial & Engineering Chemistry Fundamentals, 1979. **18**(4): p. 433-435.
95. Balasubramanian, M., A. Meisen, and K.B. Mathur, *Spouted bed collection of solid aerosols in the presence of electrical effects.* Canadian Journal of Chemical Engineering, 1978. **56**(3): p. 297-303.
96. Figureroa, A.R. and W. Licht, *Filtration of submicron particles by fixed and fluidized granular beds.* A.I.Ch.E. , 1978. **Symp. Ser. 74**(N175).
97. Liao, C.-C., S.-S. Hsiau, and T.-Y. Huang, *The effect of vibrating conditions on the electrostatic charge in a vertical vibrating granular bed.* Powder Technology, 2011. **208**(1): p. 1-6.
98. Cheng, Y., et al., *Investigation on Electrostatic Charging and Its Effect on Mixing of Binary Particles in a Vibrating Bed.* Industrial & Engineering Chemistry Research, 2014. **53**(36): p. 14166-14174.
99. Marlow, W.H. and J.R. Brock, *Calculations of bipolar charging of aerosols.* Journal of Colloid & Interface Science, 1975. **51**(1): p. 23-31.
100. Tang, M., et al., *Filtration efficiency and loading characteristics of PM2.5 through commercial electret filter media.* Separation and Purification Technology, 2018. **195**: p. 101-109.
101. Hoppel, W.A. and G.M. Frick, *Ion—Aerosol Attachment Coefficients and the Steady-State Charge Distribution on Aerosols in a Bipolar Ion Environment.* Aerosol Science and Technology, 1986. **5**(1): p. 1-21.

102. Alonso, M., A. Hernandezsierra, and F. José Alguacil, *Diffusion charging of aerosol nanoparticles with an excess of bipoloar ions.* Journal of Physics A General Physics, 2002. **35**(30): p. 6271.
103. Hogan, C.J., et al., *Estimating aerosol particle charging parameters using a Bayesian inversion technique.* Journal of Aerosol Science, 2009. **40**(4): p. 295-306.
104. Inc., T., *Instruction manual, Model 3076 Constant Output Atomizer, P/N 1933076.* 2005.
105. Kim, S.H., G.W. Mulholland, and M.R. Zachariah, *Understanding ion-mobility and transport properties of aerosol nanowires.* Journal of Aerosol Science, 2007. **38**(8): p. 823-842.
106. Pushnov, A.S., *Calculation of average bed porosity.* Chemical and Petroleum Engineering, 2006. **42**(1): p. 14-17.